ATTACHMENT 2

REPORT GA-C17128

GA Technologies

GA-C17128

SAFETY ANALYSIS REPORT FOR FUEL RELOAD 3

(SEGMENT 9 - CYCLE 4)

FORT ST. VRAIN NUCLEAR
GENERATING STATION

GA TECHNOLOGIES PROJECT 1900
MAY 1983

CONTENTS

TABLES

FIGURES

1. INTRODUCTION AND SUMMARY

This Safety Analysis Report (SAR) is prepared to obtain concurrence to operate the Fort St. Vrain Nuclear Generating Station (FSV) through the forthcoming reload cycle (Cycle 4). For this cycle, 6 of the 37 fuel regions in the core will be loaded with fresh fuel elements fabricated by General Atomic Company (GA). The introduction of new fuel elements is consistent with the fuel management program described in the Final Safety Analysis Report (FSAR). The regions to be refueled contain 203 standard fuel elements, 30 control fuel elements, one neutron source fuel element, and six bottom control fuel elements, a total of 240 elements to be replaced. The duration of Cycle 4 could be up to 300 effective full power days (EFPD).

This report contains sections describing the operating history of the reactor through April 30, 1983, the fuel system design, the nuclear design, the thermal-hydraulic design, and the safety aspects of the core during Cycle 4. Proposed changes to the Technical Specifications are presented. The planned startup program for the refueled core is also briefly described.

The replacement fuel elements feature one design change (use of H-451 graphite) relative to the fuel design described in the FSAR, the Technical Specifications, and previous reload SARs. This design change was the subject of a lengthy generic review and approval by NRC in 1978 and 1979. The safety evaluation for the change as it affects this core reload is presented in this report. No unreviewed safety questions, as defined in 10CFR50.59, are presented. None of the peak operating conditions presented in the FSAR are exceeded.

2. REACTOR OPERATING HISTORY

Initial criticality of the FSV reactor was achieved on January 31, 1974, with initial generation of electricity on December 11, 1976. Prior to February 1, 1979, when the plant was shut down for refueling, the initial core had operated a total of 174 EFPD. Cycle 2 operation began on May 26, 1979 and was completed on May 13, 1981, having accumulated a total of 189 EFPD. Cycle 3 operation began on July 15, 1981, and as of April 30, 1983, had accumulated a total of 170.5 EFPD.

The nuclear performance of the FSV core has been, in general, as predicted. Good agreement between measurements and calculations has been obtained for shutdown margins, temperature coefficients, xenon worth, and control rod worth (i.e., measurements are well within the acceptance criteria specified for the tests). Initial cold criticalities in Cycles 1-3 were predicted within 0.003 Δk. Analyses have overpredicted the end-of-cycle (EOC) reactivities of the core at operating temperatures by a few tenths of a percent; however, the difference between observed and expected reactivity has remained within the 0.01 Δk limit of Technical Specification LCO 4.1.8 throughout operation.

Fission product release to date has been very low. Measured circulating activity has been approximately a factor of 30 less than the limit provided in Technical Specification LCO 4.2.8. Measurements of plateout activity obtained after removal of the first plateout probe in November, 1981 indicate that these activity levels are also substantially below Technical Specification limits (Ref. 1).

The most unusual occurrence, to date, was the detection, initially in October 1977, of temperature fluctuations. These fluctuations affected the nuclear channels, the region exit temperatures, and the steam generator module temperatures. During fluctuations, however, the total core coolant flow and core thermal power remained essentially constant. In addition, the temperature swings during fluctuations stayed within plant operations and technical specification limits.

A comprehensive program to evaluate and resolve the fluctuation issue was begun in late 1977. This program led to installation, in November 1979, of core region constraint devices (RCDs) (Ref. 2). These devices limit the small (approximately 0.10 inch) lateral movements of fuel columns to which the fluctuations were attributed. Fluctuation testing of the core up to 100% power with RCDs installed was completed in November, 1981. No fluctuations have been detected since installation of the RCDs. The results of these tests were formally submitted to NRC in July, 1982 (Ref. 3).

The second major issue with regard to reactor operation has been the existence of discrepancies between measured and calculated region outlet helium temperatures. Significant discrepancies have been limited to regions in the northwest boundary of the core (Regions 20 and 32-37), with measured temperatures being consistently less than calculated temperatures. These discrepancies are caused by a transverse flow of relatively cool helium from the core-reflector interface along the inside of the region outlet thermocouple sleeves (Type II flow). This flow passes over the region outlet thermocouple assemblies of these regions and depresses the indicated region outlet temperature.

To compensate for these discrepancies, special operating procedures were provided which insure compliance with the original core design intent. Appropriate technical specifications were developed to govern operation with these measurement errors and were submitted to NRC in July, 1982 (Ref. 4).

On October 5, 1982 NRC issued Amendment No. 28 to the FSV Operating License. In this amendment, the NRC concluded, based upon a review of Reference 3, that the fluctuation issue is resolved. The technical specifications proposed in Reference 4 were incorporated in the operating license, and all previously imposed restrictions on reactor power level were removed.

As a result of the visual examinations conducted on fuel elements removed from the reactor during the second refueling, two Segment 2 fuel elements were each found to have one or two cracked graphite webs. The presence of these cracks did not affect the cooling geometry of the fuel or the ability of the fuel handling machine to safely remove the fuel elements from the core. PSC has kept the NRC apprised of the status of these cracked webs (Ref. 5). A DOE-funded program is being carried out at GA to investigate this issue, while a similar NRC-funded program is being conducted at Los Alamos National Laboratory.

3. GENERAL DESCRIPTION

The FSV fuel management scheme is designed so that approximately one-sixth of the core is reloaded at periodic refueling intervals. This document describes the third reload segment (also known as Segment 9) to be inserted into the FSV core. It is projected that Segment 9 will reside in the core within the 1800 EFPD limit of Technical Specification LCO 4.1.1. This reload fuel segment is designed so that the core performance with the new fuel added satisfies the reactor Technical Specifications. These limitations apply to the total core performance. That is, not only do the freshly loaded refueling regions meet power distribution limitations, but the perturbations to the remainder of the core are such that the segments remaining in the core from the previous cycle also satisfy the performance requirements. These performance requirements include core excess reactivity, shutdown margins, power distribution behavior, and all the core safety considerations discussed in the FSV FSAR.

About one-sixth of the core is replaced at each refueling. The scheduled refueling sequence is summarized in Fig. 3-1.* It can be seen that six refueling regions are reloaded at each refueling, except for the fifth reload, at which time the central refueling region is also replaced. Segment 9 consists of 203 standard fuel elements, 30 control fuel elements, one neutron source element, and 6 bottom control fuel elements. In this reload segment, three of the refueling regions are located in the central portion of the core (Regions 3, 13, and 18)

*Figures and tables appear at the end of each section.

and three are located adjacent to the side core-reflector interface (Regions 22, 29, and 33). A new neutron source will be placed in the top active core layer of Region 22 in order to assure an adequate count rate for the startup range detectors. The refueling region sequence was chosen so that freshly refueled regions are never adjacent to each other (except when Region 1, the central region, is reloaded). Therefore, each refueling region is surrounded by regions of varying ages.

Figure 3-2 shows the refueling region age distribution for the equilibrium cycle as given in FSAR Section 3.5. By comparison of this figure with Fig. 3-1, it can be seen that the reload sequence follows that given in the FSAR.

Segment 9 features one change relative to the fuel design described in the FSAR, the Technical Specifications, and previous reload SARs (Refs. 6 and 7). Because the H-327 graphite used in the inital core and in Segments 7 and 8 is no longer available, some of the fuel elements of Segment 9 (Regions 3, 13, and 18) will use H-451 graphite. The remaining fuel elements in Segment 9 (Regions 22, 29, and 33) will use the remaining stock of H-327 graphite. Use of H-451 graphite requires a change to Technical Specification DF6.1, as discussed in Section 8.0 of this report.

Use of H-451 graphite in FSV reload segments was the subject of a lengthy generic review and approval by NRC in 1978 and 1979 (Refs 8 - 16). As a result of that review, NRC concluded that substitution of H-451 for H-327 graphite elements in FSV would result in negligible changes in the nuclear and thermal behavior of the core and would not result in reduced safety margins or reliabililty compared to the reference H-327 core (Ref. 16). It was also concluded by NRC that the

information provided to NRC by GA during that review may serve as an acceptable reference and the initial basis for allowing the substitution of H-451 graphite fuel and reflector elements for the reference H-327 elements.

It was also noted by the NRC in Reference 16 that a final decision to use H-451 graphite in FSV would be based upon an NRC review of an application from Public Service Company of Colorado describing the exact composition of any reload fuel utilizing H-451. It was also required in Reference 16 that, as part of any application for insertion of H-451 reload elements, reports be provided on the results of the ongoing irradiation creep program and on post-irradiation examinations of the H-451 fuel test elements, which were inserted in FSV during the first refueling. Information on graphite creep and on the examination of test element FTE-1, the only test element using H-451 graphite removed from the reactor to date, was provided to NRC by PSC in Reference 17.

This Safety Analysis Report provides specific information on the reload fuel which will utilize H-451 graphite and provides the safety evaluation in support of the change to Technical Specification DF6.1. Extensive reference is made to the information in References 8 - 16.

As shown in the subsequent sections of this report, evaluations of this design change have shown that it has no adverse impact upon core performance or plant safety. Accordingly, it presents no unreviewed safety questions as defined in 10CFR 50.59.

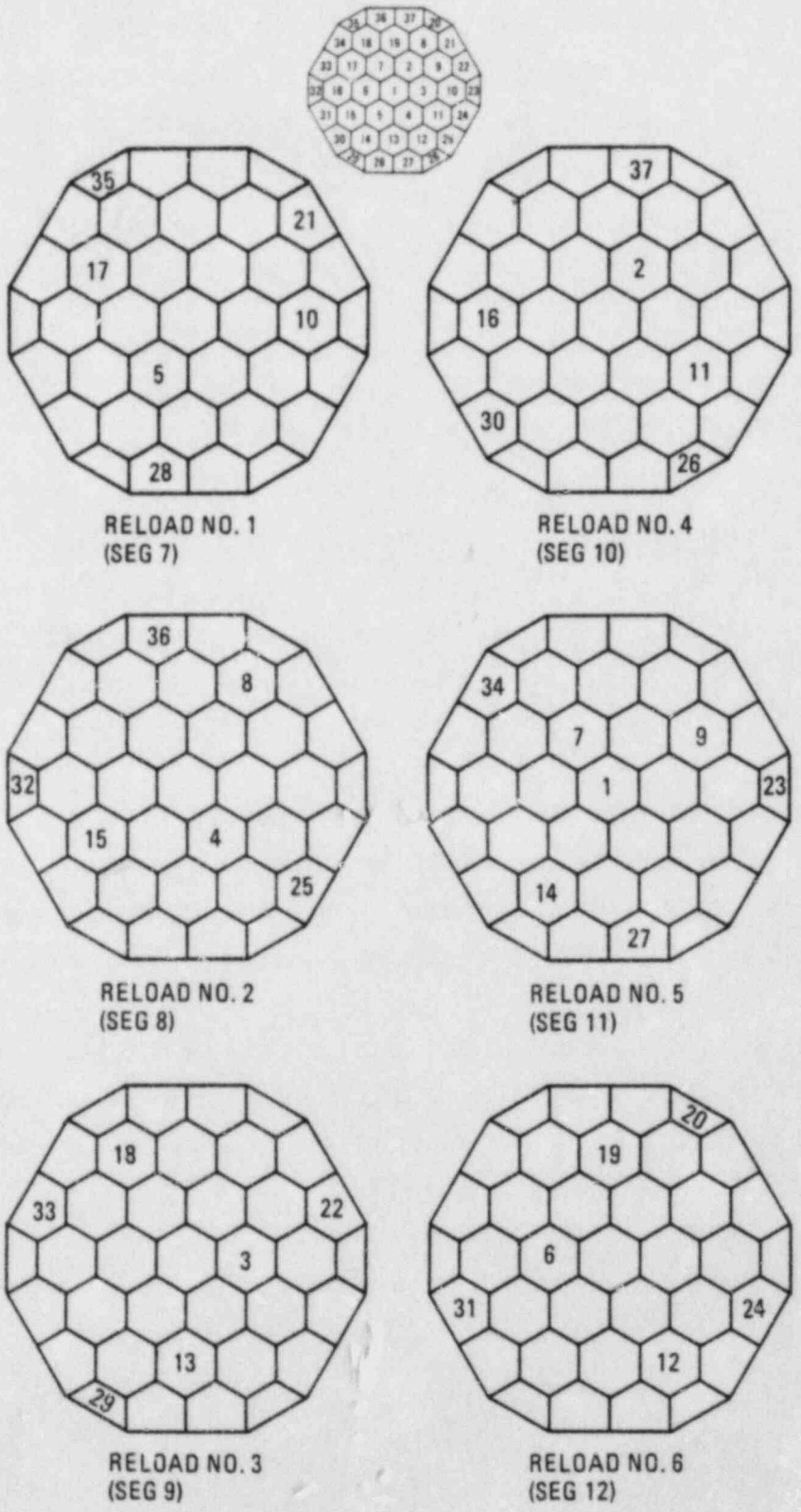

Fig. 3-1. Core regions refueled in reloads 1 through 6

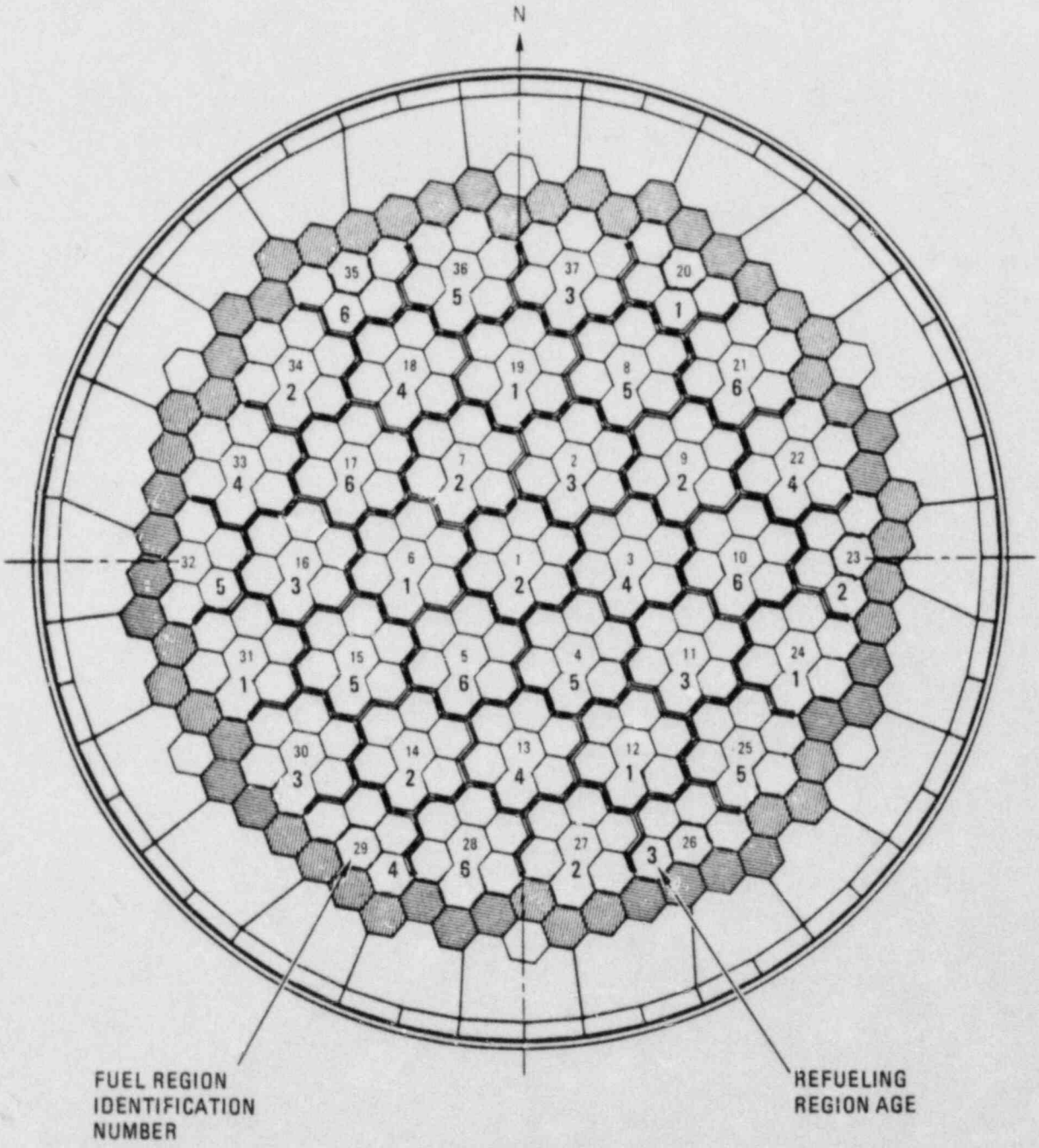

Fig. 3-2. Refueling region age distribution for the equilibrium cycle (before refueling)

4. FUEL SYSTEM DESIGN

4.1 FUEL DESIGN

The fuel elements in this third reload are, except for the use of H-451 graphite, of the same basic design as those in the initial core and Segments 7 and 8. TRISO-coated $(Th/U)C_2$ and ThC_2 particles are bonded by a carbonaceous matrix into fuel rods which are cured and loaded into graphite fuel blocks. The configuration of these fuel elements is identical to that used in Segments 1-8. The materials and processes used in manufacture are essentially the same as those for the initial core fuel elements or for previous reload fuel elements (Refs 6 and 7). Fuel and burnable poison loadings have been adjusted to accommodate the reactivity requirements of the cycle, as discussed in Section 5.

As was shown in References 8-16, H-451 graphite is a better structural material than H-327 graphite due to its near-isotropic nature, its lower irradiation-induced axial dimensional changes, and its higher strength. The effects of the use of H-451 graphite on core performance are discussed in subsequent sections. Although this design change requires a change to the Technical Specifications, as shown in the following sections it does not involve any unreviewed safety questions as defined in 10CFR50.59.

4.2 MECHANICAL DESIGN

The fuel elements for Segment 9 of the FSV core are fabricated from both H-327 and H-451 graphite. The configuration of these fuel

elements is identical to that used in Segments 1 through 8. Table 4-1 provides a summary of the Segment 9 fuel element stress, strain, and bowing analyses described in this section.

Stress analysis was performed for the FSV Segment 9 fuel elements (both H-451 and H-327 graphite) using the methods discussed in the FSAR. Operating and shutdown strain and stress distributions were calculated for the axial and radial orientations thoughout the lifetime of the fuel elements. All operating and shutdown stresses were less than those predicted for the initial core fuel elements (FSAR Section 3.4.2.1.1) except for the radial operating stress in one core location. In this location, the control column of Region 13, a maximum radial stress of 217 psi was calculated - a value which is 8.5% higher than the FSAR peak value. However, the fuel blocks in Region 13 will be made from H-451 graphite. As discussed in Reference 8, the radial strength of H-451 graphite is 66% higher than that of H-327 graphite. Therefore, despite the 8.5% higher calculated stress in Region 13, which results from the higher Young's modulus of H-451 graphite (Ref. 8), a larger design margin exists than would have been obtained with the use of H-327 graphite. This result is consistent with the conclusions reached in References 8-16.

During core operation, the Segment 9 fuel elements will be exposed to fast neutron irradiation, which will induce dimensional changes in the graphite. An analysis was performed to calculate the expected dimensional changes of the Segment 9 fuel elements. The maximum axial dimensional changes of all Segment 9 fuel columns were less than those of the initial core fuel columns shown in FSAR Section 3.4.2.1.2. The maximum calculated EOL bowing for the buffer elements is 0.09-in., which was the maximum bowing predicted for the initial and equilibrium core H-327 buffer elements (FSAR, Section 3.4.2.1.2).

4.3 THERMAL DESIGN

The selection of fuel rod and burnable poison loadings and of the control rod program for Cycle 4 (see Section 5) is made so that the Cycle 4 power distribution falls within the limits described in the FSAR. No changes are planned for the operation of the core cooling during Cycle 4 (i.e., helium temperature at the core inlet and average outlet temperature will be enveloped by the FSAR reported values).

Accordingly, the temperature limits presented in the FSAR will not be exceeded during Cycle 4. This conclusion is supported by analyses using the COPE code (Ref. 18), which is discussed in the FSAR. The results of these analyses are also shown in Table 4-1.

Introduction of H-451 graphite in the fuel design for Segment 9 results in increased graphite thermal conductivity. The increased thermal conductivity results in a smaller temperature rise across the graphite web and in lower fuel centerline temperature than would be obtained using H-327 graphite. Reductions in fuel temperature will lead to lower kernel migration rates and a resulting increased margin relative to the core thermal safety limit (Ref. 8).

4.4 FISSION PRODUCT RELEASE

During Cycle 4, the FSV core is expected to be operated within the limits presented in the FSAR and contained in the Technical Specifications. Accordingly, the fission product release characteristics of the fuel are expected to be within design limits, and the design radionuclide inventories presented in Section 3.7 of the FSAR will not be exceeded. These conclusions are consistent with operating experience gained during Cycles 1-3.

As discussed in References 8-16, the release of noble gas and gas-like (Se, Te, I) fission products is expected to be reduced with the use of H-451 vs H-327 graphite in the core. The reduction in gaseous fission product release will result from the lowering of fuel temperature discussed in Section 4.3 and its effects on R/B, the gaseous fission product release-to-birth rate ratio in the fuel.

Negligible changes in the release of metallic fission products are expected due to the decreases in fuel temperature. As discussed in References 8-16, the available data indicate that the sorptivity and diffusivity of elements such as strontium are essentially the same for both H-327 and H-451 graphites. Hence, changes in graphite type will not affect the release of metallic fission products.

Thus, the circulating and plateout activity source terms presented in Tables 3.7-1 and 3.7-2 of the FSAR remain appropriate for use in FSV accident analyses.

TABLE 4-1
SEGMENT 9 CALCULATED PEAK OPERATING CONDITIONS VERSUS
FSAR INITIAL CORE PEAK VALUES

Parameter	FSAR Peak Value	Segment 9 Peak Value[a]
Axial operating stress (psi)	450	324
Radial operating stress (psi)	200	217[b]
Initial axial thermal stress (psi)	150	64
Initial radial thermal stress (psi)	180	117
Column axial strain (%)	2.1	1.8
Buffer element bowing (in.)	0.09	0.09
Fuel temperature (^{o}F)	2300	2148[c]

(a) Values calculated using FSAR methods.

(b) See discussion in Section 4.2.

(c) Peak fuel temperature in core during Cycle 4.

5. NUCLEAR DESIGN

5.1 SEGMENT 9 FUEL LOADING

In the initial core design, the fuel was zoned both radially and axially to achieve the desired power distribution and to mock up the equilibrium cycle. The core was divided into four radial zones and two axial zones. The radial zones consisted of the central refueling region, the six refueling regions adjacent to the central regions, the 12 refueling regions adjacent to these six regions, and the outer 18 refueling regions adjacent to the side reflector. In addition, the five rows of fuel rods in the outer 18 regions that were immediately adjacent to the side reflector interface contained a buffer fuel loading with low uranium and high thorium loading to reduce the power peaking at the reflector edge. There were two axial zones consisting of the top and bottom three layers of fuel elements. The buffer zone was not axially zoned. These various fuel zones, combined with a partial mock-up of the equilibrium core fuel distribution, made it necessary to fabricate 13 different fuel blends or compositions for the initial core fuel elements.

For the design of the reload segments, these different fuel zones are essentially maintained, except that the second and third radial zones are combined and the width of the buffer zone is increased to the width of a fuel element. Since the central refueling region is not reloaded in this reload segment, only six new fuel compositions or blends (numbered 26 through 31) are used for the Segment 9 fuel. Refueling regions 3, 13, and 18 require a top and bottom fuel loading, and refueling regions 22, 29, and 33 require a top and bottom fuel loading. In addition, two loadings are required for the buffer fuel at the core-side reflector interface, which is axially zoned as it was in Segment 8 (Ref. 7).

A summary of the 6 different fuel blend uranium and thorium loadings used for the third reload segment is given in Table 5-1. Fuel blends 26 and 27 are used in the inner refueling regions, and blends 28, 29, 30, and 31 are used in the outer refueling regions. Blends 30 and 31 are used in the buffer zone.

In addition to the six new fuel blends for Segment 9 discussed above, one spare Segment 7 fuel element will be used in Segment 9. This spare Segment 7 fuel element is a standard element containing blend 14 fuel in an H-327 graphite body. As shown in Table 5-2, in which heavy metal loadings of blend 14 fuel are compared with those of Segment 9 blends, the blend 14 loadings are closest to the loadings of blend 30 in Segment 9. Blend 30 is used in the upper half of the buffer fuel zone. Accordingly, the spare Segment 7 fuel element will be located in the buffer zone in the top active core layer. Since the heavy metal loading of the spare Segment 7 element is slightly lower than the blend 30 element it replaces, its power generation will be slightly lower. The resulting change in power peaking factors has been shown to be negligible, and the effect on core reactivity has been shown to be undetectable within the precision of the design methods. By placing the spare Segment 7 element in the top active core layer, perturbations upon fuel performance will be further minimized, since fuel temperatures at this location are the lowest in the core. Furthermore, by placing the spare Segment 7 element in the buffer zone, it will be mixed with other fuel elements that have H-327 graphite bodies. This placement is consistent with the statement in Reference 8 that any axial layer within a region will be composed of the same type of graphite.

It is anticipated that the reactor will have operated for up to 663 EFPD, generating a total of up to 1.3×10^7 MW-hr of energy at the time

of the third refueling. The projected heavy metal loadings in the remaining core segments at the EOC 3 (663 EFPD) are given in Table 5-3. The maximum burnup in fissile particles is projected to be about 14.0% FIMA and in fertile particles about 2.0% FIMA. These burnups are substantially lower than the limiting values given in the FSAR, Appendix A, Table A.1.1-2. The maximum projected fast flux (E > 0.18 MeV) exposure in the discharged segment is about 3.2×10^{21} nvt.

5.2 BURNABLE POISON LOADING

Six holes are provided in each standard fuel element, one at each corner, for insertion of burnable poison rods; four holes are provided in each control fuel element. For Segment 9 fuel, there will be no burnable poison in the control fuel elements; all six poison holes in the standard elements may be used depending on burnable poison loading requirements.

In the initial core and Segment 7, different poison rod types, varying in their boron loading, were used to provide reactivity control and to adjust power distributions in fresh fuel regions. The poison rods were 28.5 inch long. In the case of Segment 7, it was necessary to have available several different poison rod types, only two of which were ultimately used. The poison rods to be used were chosen based on the reactivity requirements of the core at the EOC 1 and were inserted into the reload segment just prior to refueling.

To avoid this unnecessarily complex and costly procedure, the design of the poison rods was slightly changed for Segment 8 and later segments (Ref. 7). Instead of using single rods 28.5 inch long, shorter rods (1.98 inch long) are loaded into the poison holes in combination with graphite dummy spacer rods (also 1.98 inch long). Each poison hole

either contains 14 poison rods, a combination of 14 poison rods and spacers, or is left empty. The boron loading in each element is controlled by varying the combination of poison rods and spacers. The new poison rods are the same in diameter (0.45 inch) and made of the same graphite as the 28.5 inch single rods previously used. The spacer rods are also 0.45 inch in diameter and are made of HLM graphite. This change does not require any changes to the Technical Specifications, nor does it constitute a change to the core design as described in the FSAR.

For Segment 9, 28.5 inch poison rods left over from Segment 7 will be cut into 1.98 inch nominal length rods and loaded into the standard fuel elements in combination with graphite spacers. The poison rods left over from Segment 7 which will be used in Segment 9 are known as "type 6" and "type 9" rods. They differ only in their boron loadings. The standard fuel elements in the upper core half will be loaded with 14 poison rods in each of the six poison holes. In the lower core half, each of the six poison holes in the standard fuel elements will be loaded with five poison rods, four spacer rods, and five more poison rods, in that sequence. The poison holes in the control fuel elements will be left empty. The use of burnable poison rods in Segment 9 is summarized in Table 5-4, and the loading sequence for the type 6 and type 9 rods is shown in Fig. 5-1.

The burnable poison loading for Segment 9 described above was used for the Cycle 4 depletion analyses referred to in the following sections. This loading will be used in Segment 9 unless the reactivity characteristics of the core or the length of Cycle 3 deviate significantly from current projections.

5.3 CONTROL ROD SEQUENCE

Technical Specification LCO 4.1.3 states that a control rod sequence will be specified for each fuel cycle and that the sequence will always be followed, except for rod insertion resulting from a scram or rod runback or during low-power physics testing. The control rod sequence for use during Cycle 4 is given in Table 5-5. The identification of the control rod groups is shown in Fig. 5-2.

The regulating rod is located in the central refueling region (rod group 1). This group is partially withdrawn before criticality is achieved and then maintained in its most reactive control rod position for the remainder of the operation. In this manner, minor reactivity adjustments can be made most rapidly with the minimum amount of control rod motion. This is consistent with the method of operation utilized for the control rods in previous cycles.

A summary of the calculated power peaking factors obtained using the control rod sequence for all control rod configurations is given in Table 5-6. This includes all of the control rod configurations in which the control rod groups are either fully inserted or withdrawn, including those subcritical configurations during the withdrawal of the first few control rod groups. Any configuration with a partially inserted control rod group will have peaking factors lying between those calculated when that group is fully inserted and fully withdrawn. The control rod worths and power peaking factors in Table 5-6 were calculated at the beginning of cycle (BOC) with equilibrium xenon (5 EFPD). Rod worths at middle of cycle (MOC) and EOC will be essentially unchanged from those given in the table. Power peaking factors during Cycle 4 depletion are discussed in Section 5.4.

The control rod configurations shown in Table 5-6 may be separated into four categories of reactor power operation: (1) full power, (2) 20% to 100% power, (3) 0% to 20% power, and (4) subcritical. Full-power operation may be achieved with configurations ranging from one control rod group (three rod pairs) fully or partially inserted at the EOC 4, when the excess reactivity is relatively low, to three control rod groups (nine rod pairs) fully or partially inserted at the BOC 4, when fission product poisons such as xenon are not present. (Except as allowed by Technical Specification LCO 4.1.4, only one control rod group in addition to group 1, the regulating rod, will be partially inserted at any time.)

At less than full power, in the range of exit gas temperatures between 1460° and 950°F, when the xenon level and the core temperature are lower, configurations ranging from four control rod groups (12 rod pairs) to five control rod groups (15 rod pairs) fully or partially inserted can be expected, depending on the temperature, power level, and the rate at which power was increased from the previous level.

The third category covers the rise-to-power phase from the cold critical condition to about 20% power (gas outlet temperatures $\lesssim$950°F). Different limiting operating conditions are applied to this phase of reactor operation by the Technical Specifications. The initial cold criticality, following the refueling operation, was calculated to be achieved with seven rod groups (21 rod pairs) fully inserted, the regulating rod 115 in. withdrawn, and control rod group 2 95 in. withdrawn.

The last category covers the subcritical control rod configurations where region peaking factors (RPF) or intraregion tilts are not meaningful, and consequently, are not given in Table 5-6.

From the data given in Table 5-6, it can be seen that the calculated power peaking factors for the various power levels do not exceed those given in Technical Specification LCO 4.1.3. This is true for both the radial region peaking factors and the intraregion peaking (column tilt) factors. The radial region peaking is below 1.83 for all configurations involving less than 19 control rod pairs. For low-power operation (gas outlet temperature $\leq 950^{\circ}F$), when more control rod pairs are inserted, the region peaking is below 3.0 until the subcritical configurations are reached. In the same manner, the intraregion peaking factors are also acceptable. It is clear, therefore, that use of H-451 graphite has no adverse impact on power peaking factors, a result which is consistent with the conclusions of References 8-16.

5.4 PROJECTED CYCLE 4 OPERATION

This section presents the results of Cycle 4 depletion analyses using design methods discussed in Section 3.5 of the FSAR. Fuel and burnable poison loadings discussed previously were used as input (see Sections 5.1 and 5.2).

Figures 5-3a through 5-3c present envelopes encompassing projected RPFs and column tilts during Cycle 4 depletion. The results indicate that RPFs and tilts during Cycle 4 will be well within the allowable limits set by LCO 4.1.3 and that the use of H-451 graphite has no adverse impact on radial power distributions. This result is consistent with the conclusions of References 8-16.

Axial zoning of the Segment 9 fuel and burnable poison is provided (1) to produce a power distribution which tends to reduce axial fuel temperature peaking and (2) to maintain the desired axial power

distribution with depletion. The calculated axial power factors in the bottom layer of each fuel region during Cycle 4 are shown in Table 5-7. The calculations were carried out with the GATT code, the three-dimensional whole core model which is used in the semi-annual fuel accountability analyses. It can be seen that the LCO 4.1.3 limits on peaking factor in the lower fuel layer are not exceeded and that the use of H-451 graphite does not result in unacceptable axial power peaking, as was also concluded in References 8-16.

The basis of Technical Specification LCO 4.1.3 also states that an acceptable flux distribution shall be maintained at lower power levels by keeping the flux level in the center of the core at least as high as the average level. Table 5-8 shows the ratio of the flux in the inner core regions (Regions 1-19) to the core average flux for each of the three control rod configurations in Table 5-6 which can result in operation between 0% and 20% power during Cycle 4. The flux ratio is above 1.0 for all cases, consistent with the basis of LCO 4.1.3.

5.5 MAXIMUM CONTROL ROD WORTH

The basis of Technical Specification LCO 4.1.3 states that the accidental removal of the maximum worth single rod pair shall result in a transient with consequences no more severe than the withdrawal of 0.012 Δk, at rated (i.e., 100%) power, from a core which has a temperature defect between 220°F and 1500°F of 0.028 Δk. In addition, the calculated worth of any rod pair in any configuration with the reactor critical must be less than 0.047 Δk. The rod withdrawal accident (RWA) at full power evaluated in Section 14.2 of the FSAR assumes withdrawal of a control rod worth of 0.012 Δk at equilibrium EOC with an equilibrium EOC temperature defect of 0.028 Δk. The consequences of withdrawal of this 0.012 Δk EOC control rod, because of the lower

reactivity feedback at EOC resulting from the less negative temperature coefficient at EOC, are equivalent to the consequences of withdrawal of a rod worth of about 0.016 Δk at BOC. Because the consequences of an RWA are a function of rod worth, steady-state core temperature (i.e., initial power level), and temperature coefficient (which varies slightly with burnup during the cycle), it is necessary to evaluate control rod worth as a function of control rod insertion.

The control rod withdrawal sequence for Cycle 4 was described in Section 5.3. For this sequence the maximum control rod worths are shown in Table 5-6. These rod worths were calculated for the core with equilibrium xenon at the beginning of Cycle 4. Additional calculations indicate that these maximum rod worths do not change significantly with burnup during the cycle. As discussed in Section 5.3, the control rod configurations shown in Table 5-6 may be divided into four categories of reactor power operation: (1) full power, (2) 20% to 100% power, (3) 0% to 20% power, and (4) subcritical.

The results in Table 5-6 indicate that the maximum worth rod pair in any critical configuration during Cycle 4 is 0.026 Δk, which is less than the 0.047 Δk limit of LCO 4.1.3.

Table 5-6 also indicates that during Cycle 4 at full power, with two control rod banks fully inserted, a maximum control rod worth of about 0.013 Δk is obtained, which is larger than the 0.012 Δk rod worth evaluated in the FSAR for an EOC rod withdrawal accident. It is, however, very unlikely that the reactor could be operated at the end of Cycle 4 at full power with two rod banks fully inserted. Analyses with the GAUGE code indicate that at EOC, even with Pa-233 or xenon fully decayed, the reactor would have to operate at less than 70% power to be

critical with two banks fully inserted. The consequences of an RWA at this lower power level are less severe than those discussed in the FSAR. Early in Cycle 4, when the reactor can be critical at full power with two rod banks fully inserted, the consequences of an RWA at full power are also less severe than those discussed in the FSAR. This result is to be expected since, as described above, a maximum rod worth of 0.016 Δk at BOC is equivalent to a maximum rod worth of 0.012 Δk at EOC with regard to RWA consequences, and the 0.013 Δk maximum rod worth for Cycle 4 is within this BOC value.

As stated above, it is very unlikely that the reactor could be critical at 100% power at end of Cycle 4 with two control rod banks fully inserted. Full power criticality at EOC with this rod configuration could be attained only if the reactor power were increased very rapidly from zero to 100% power (no xenon buildup) following a prolonged shutdown (all Pa-233 decayed). Plant operating requirements (steam generator boilout, turbine warming, etc.) preclude this situation. Nevertheless, the consequences of an 0.013 Δk RWA at full power end of Cycle 4 were evaluated using the Cycle 4 power distributions discussed in Section 5.4 and the Cycle 4 kinetics parameters presented in Section 5.7. The evaluation was performed with the same methods (the BLOOST code) used in the FSAR RWA analyses.

The results of these RWA evaluations indicate that the consequences of accidental withdrawal of a 0.013 Δk control rod at end of Cycle 4 are the same or less than those for the equilibrium core RWA discussed in the FSAR. This result is obtained because the region peaking factors expected to occur during Cycle 4 are somewhat smaller than those assumed for the FSAR analysis and because Cycle 4 kinetics parameters are somewhat less severe than those for the equilibrium core. Fuel

temperature in an average power channel is expected to increase by about 400°C for both RWA cases. Fuel temperature in the hottest channel is expected to increase only about 900°C for the Cycle 4 RWA, vs. about 1800°C for the FSAR case.

Table 5-6 also indicates that with five or six rod banks fully inserted a maximum control rod worth of 0.015 Δk is obtained. Reactor criticality with this control rod configuration can be obtained at EOC only at very low (a few percent) power. At BOC criticality may occur with that configuration at full power. However, this 0.015 Δk rod worth is less than the 0.016 Δk rod worth evaluated in the FSAR for a rod withdrawal accident at BOC.

Therefore, it can be seen that the use of H-451 graphite has no adverse impact upon control rod worths or upon the consequences of postulated rod withdrawal accident. This result also is consistent with conclusions reached in References 8-16.

5.6 CORE SHUTDOWN MARGIN

Technical Specification LCO 4.1.2 requires that the reactor be capable of being shut down (at least 0.01 Δk subcritical) with any one control rod pair withdrawn at room temperature. This is consistent with the assumption that, during the rod withdrawal accident postulated in Section 14.2 of the FSAR, the control rod pair being withdrawn is continuously withdrawn until fully removed during the accident and is not capable of being reinserted. The reactor design criteria require that the reactor be capable of being shut down at refueling temperature with any two control rod pairs inoperable for up to two weeks. The requirement for being shut down with any two control rod pairs withdrawn is established to allow for operation with one inoperable control rod

pair. In addition, LCO 4.1.2 requires that cold shutdown be achievable prior to Pa-233 decay with any two rod pairs, or with any two adjacent rod pairs plus a third rod pair that is at least three regions away from the two unrodded regions, removed.

The net negative reactivity insertions following a scram during Cycle 4 are shown in Table 5-9. Excess reactivity during Cycle 4 is projected to vary from 0.053 Δk at BOC, to 0.029 Δk at MOC, to 0.014 Δk at EOC, based up GAUGE code analyses.[1] Thus the minimum instantaneous shutdown margin during Cycle 4 is obtained at BOC with the two maximum worth rods inoperable: 0.082 Δk. This shutdown margin is reduced after shutdown due to core cooling (in a matter of hours), due to xenon decay (in a matter of a few days), and due to decay of Pa-233 to U-233 (in a matter of weeks).

To show that the shutdown margin is satisfactory for these cases with one or more control rod pairs assumed inoperable, the summary in Table 5-10 gives calculated core shutdown margins at BOC immediately after refueling (5 EFPD) and at MOC and EOC. It can be seen that for all of the various cases of interest, the shutdown margin is larger than 0.01 Δk, as required in the Technical Specifications and reactor design criteria. Accordingly, the use of H-451 graphite has no adverse impact upon shutdown margins. This result is also consistent with the conclusions reached in References 8-16.

---

[1] As noted in Section 2, core reactivity has been overpredicted during Cycles 1-3 by a few tenths of a percent. If this trend continues, as expected, during Cycle 4, shutdown margins will be larger than those calculated in this section by the same amount.

For the case with only the maximum worth rod pair inoperable, the minimum shutdown margin at room temperature with xenon and Pa-233 decayed (the most reactive case) is 0.042 Δk, which is obtained at BOC (5 EFPD). At refueling temperature (220°F), this value would be 0.048 Δk for the same condition. However, since the second maximum worth rod out can add as much reactivity as 0.040 Δk, it would not be possible to maintain a shutdown margin of 0.01 Δk with these two rod pairs out if the Pa-233 is allowed to fully decay to U-233. This situation does not conflict with the LCO, however, since the requirement for the two rod pairs out at refueling temperature is established to allow for operation with one inoperable control rod drive assembly. An adequate shutdown margin can be maintained for a period of at least two weeks in this core condition. If the inoperable unit cannot be repaired in this time period, the reserve shutdown system can be used to maintain adequate reactivity control. The occurrence of this minimum shutdown margin at BOC is primarily due to the unusually long shutdown for refueling that was assumed in these analyses (60 days instead of the 14 days assumed in FSAR analyses). As a result of this conservative assumption most of the Pa-233 present at end of Cycle 3 is decayed to U-233 at beginning of Cycle 4, thereby reducing the shutdown margin. Furthermore, the probability of having two inoperable control rods at BOC is quite small since the shutdown time between Cycles 3 and 4 provides ample opportunity to confirm that all control rod drives are in working order.

General requirements for operability of control rod drives during the cycle are provided in Technical Specification LCO 4.1.2.

5.7 KINETICS PARAMETERS

The kinetics parameters for Cycle 4 as well as for the initial and equilibrium cycles (taken from the FSAR) are given in Table 5-11. The data in this table indicate that the equilibrium cycle kinetics parameters represent a conservative estimate of the Cycle 4 kinetics. The Cycle 4 kinetics parameters were used in the RWA analyses described in Section 5.5.

Technical Specification LCO 4.1.5 requires that the reactivity change due to an average core temperature increase between 220°F and 1500°F (refueling temperature to rated power conditions) in the absence of xenon must be at least as negative as 0.031 Δk. This requirement is imposed because FSAR accident analyses assumed a temperature defect of 0.028 Δk and the uncertainty in measured temperature defect is about $\pm$ 10%, or about 0.003 Δk. The temperature defect measurements required by Technical Specification SR5.1.3 have confirmed that the agreement between measured and calculated temperature defect is within $\pm$ 10%.

The calculated temperature defect at the beginning and at the end of Cycle 4 is shown in Figure 5-4. The results indicate that the temperature defect between average core temperatures of 220°F and 1500°F is 0.044 Δk at BOC and 0.031 Δk at EOC. Both of these calculated values meet the requirement of LCO 4.1.5 for measured temperature defect.

Certain conservatisms were employed in the calculation of these temperature defects such that expected values are larger than those presented in Figure 5-4. It was assumed that the core is in the cold critical condition and that control rods are then removed to achieve a higher power level and fuel temperature. Since some power is being generated in this scenario, it is inevitable that some buildup of xenon

occurs. The presence of xenon tends to decrease the calculated temperature defect. Therefore, the temperature defects in the absence of xenon, the limit on which is specified in LCO 4.1.5, will be larger than the values shown in Figure 5-4.

From the results presented in this section, it can be seen that use of H-451 graphite has no adverse impact upon kinetics parameters, another result consistent with the conclusions of References 8-16.

5.8 ANALYTICAL INPUT

Nuclear analyses were carried out using the same methods applied to the analyses presented in the FSAR, previous reload SARs, and the semi-annual fuel accountability reports. The design of Segment 9 introduces no new aspects to high-temperature gas-cooled reactor (HTGR) core design techniques; consequently, there was no need to develop or adapt any new methods or procedures for the nuclear design.

The depletion analyses described in this chapter were performed by simulating the actual core power history for Cycles 1 and 2 and the first 150EFPD of Cycle 3. Continuous operation at 70% power for the balance of Cycle 3 and at 100% power for Cycle 4 was assumed. Cycle 3 was assumed to continue to a total length of 300 EFPD. Cycle 4 was assumed to be 300 EFPD in length.

5.9 CORE OPERATING PROCEDURES

Core operating procedures will be the same as those for previous cycles and those planned for equilibrium cycles. The only differences will be the control rod withdrawal sequence discussed in Section 5.3 and the use of comparison regions as described in Reference 4 and required by Amendment No. 28 to the FSV Operating License.

TABLE 5-1

FSV RELOAD 3 (SEGMENT 9) AS BUILT FUEL LOADINGS

Fuel Blend	Uranium Loading gm/rod	Uranium Loading Total(kg)	Thorium Loading gm/rod	Thorium Loading Total(kg)
26	0.349	64.6	3.46	640.7
27	0.212	39.0	2.80	514.4
28	0.430	36.9	3.52	302.2
29	0.258	21.9	2.92	247.9
30	0.323	26.0	3.98	320.4
31	0.194	15.5	3.11	248.9
Total		203.9		2274.6

TABLE 5-2

COMPARISON OF BLEND 14 AND SEGMENT 9 BLEND

URANIUM AND THORIUM LOADINGS

Segment 9 Blend	Blend 14 Difference, %* Uranium	Thorium
26	-15	+ 3
27	+30	+22
28	-42	+ 1
29	+15	+18
30	- 7	-12
31	+34	+23

---

* $\left(\frac{\text{Blend 14 - Segment 9 Blend}}{\text{Segment 9 Blend}} \right) \times 100\%$

TABLE 5-3

PROJECTED CORE LOADINGS AT THE END OF CYCLE 3[a]

Nuclide	Nuclide Weight (kg)/Segment						Total Nuclide Weight(kg)
	3[b]	4	5	6	7	8	
Th-232	2546.9	2337.8	2807.6	2335.3	2225.2	2252.2	14505.0
Pa-233 + U-233	42.7	41.4	49.5	41.6	33.8	25.7	234.8
U-234	4.0	4.2	4.9	4.2	3.0	2.2	22.5
U-235	44.6	50.9	56.4	50.7	87.5	116.5	406.6
U-236	13.2	15.8	17.5	15.8	15.5	11.9	89.7
U-238	6.6	7.7	8.6	7.7	9.9	10.5	51.1
Np-239 + Pu-239	0.16	0.19	0.21	0.19	0.25	0.26	1.25
Pu-240	0.06	0.08	0.09	0.08	0.09	0.07	0.46
Pu-241	0.06	0.07	0.08	0.08	0.07	0.04	0.41

(a) 663 EFPD

(b) This segment is discharged

TABLE 5-4

USE OF BURNABLE POISON IN SEGMENT 9

	Upper Core Half[a]	Lower Core Half[b]
B^{nat}, g/cm^3 (type 6 LBP rods)	0.0215	0.0215
B^{nat}, g/cm^3 (type 9 LBP rods)	0.0336	0.0336
Nominal rod diameter, in.	0.45	0.45
Nominal rod length, in.	1.98	1.98
Rods/standard element (type 6)	42	30
Rods/standard element (type 9)	42	30
Rods/control element	0	0

(a) Fuel blends 26, 28, and 30, and the spare Segment 7 (blend 14) element.

(b) Fuel blends 27, 29, and 31.

TABLE 5-5

CONTROL ROD SEQUENCE FOR CYCLE 4

Sequence	Group Withdrawn	Regions
1	2A(a)	2,4,6
2	4F(a)	25,31,37
3	4D	23,29,35
4	1(115" out)	1
5	4B	21,27,33
6	2B	3,5,7
7	4E	24,30,36
8	4A	20,26,32
9	4C	22,28,34
10	3C	10,14,18
11	3A	8,12,16
12	3B	9,13,17
13	3D	11,15,19
14	1(fully out)	1

(a) Rod groups used for rod runback.

TABLE 5-6

CALCULATED CONTROL ROD GROUP WORTH AND POWER PEAKING FACTORS WITH CYCLE 4 ROD SEQUENCE

(BOC, EQ. XE, 5EFPD)

Control Rod Configuration Rods Inserted		Group Worth Δk	Cumulative Worth Δk	Maximum RPF[a]	Maximum Tilt[b] Rodded	Maximum Tilt[b] Unrodded	Maximum Worth Rod Worth Δk	Reg
No Rods In		0.0000	0.0000	1.38	____	1.26	____	____
1 Rod (1 half in)	1[d]	0.002	0.002	1.32	____	1.25	0.002	1
4 Rods (+ 3D)[c]		0.017	0.019	1.52	1.19	1.24	0.008	15
7 Rods (+ 3B)		0.021	0.040	1.47	1.18	1.21	0.013	9
10 Rods (+ 3A)		0.014	0.054	1.69	1.31	1.29	0.012	9
13 Rods (+ 3C)	2	0.020	0.074	1.54	1.25	1.23	0.012	18
16 Rods (+ 4C)		0.012	0.086	1.65	1.31	1.24	0.015	8
19 Rods (+ 4A)	3	0.008	0.094	2.03	1.54	1.38	0.015	15
22 Rods (+ 4E)		0.010	0.104	2.69	1.60	1.32	0.014	13
25 Rods (+ 2B)		0.033	0.137	1.80	1.38	1.36	0.026	22
28 Rods (+ 4B)	4	0.012	0.149	____	____	____	____	____
28 Rods (1 fully in)		0.004	0.153	____	____	____	____	____
31 Rods (+ 4D)		0.004	0.157	____	____	____	____	____
34 Rods (+ 4C)		0.012	0.169	____	____	____	____	____
37 Rods (+ 2A)		0.046	0.215	____	____	____	____	____

NOTE: Initial criticality at 0 days was calculated with bank 2B withdrawn 95 in.

(a) RPF = region peaking factor = region power/core average region power.
(b) TILT = column peaking factor/RPF.
(c) Refers to rod group sequence (4 rods = rod 1 + group 3D).
(d) Power range defined in Section 5.3.

TABLE 5-7 (Sheet 1 of 2)
SUMMARY OF CONTROL ROD INSERTIONS AND AXIAL POWER FACTORS IN BOTTOM FUEL LAYER

	CYCLE	4		4		4		4		4	
	EFPD	5.0		50.0		100.0		150.0		155.0	
REGION	*										
1		2	.838	2	.826	2	.847	2	.848	2	.831
2		0	.778	0	.763	0	.784	0	.784	0	.760
3		0	.740	0	.721	0	.737	0	.734	0	.720
4		0	.727	0	.717	0	.738	0	.741	0	.719
5		0	.737	0	.724	0	.746	0	.746	0	.725
6		0	.790	0	.774	0	.795	0	.794	0	.772
7		0	.786	0	.771	0	.791	0	.789	0	.762
8		0	.697	0	.689	0	.714	0	.717	0	.700
9		3	.913	3	.893	3	.910	3	.906	0	.691
10		0	.695	0	.681	0	.701	0	.701	0	.695
11		6	.686	6	.681	6	.705	6	.708	3	.905
12		0	.748	0	.750	0	.779	0	.787	0	.770
13		3	.854	3	.850	3	.878	3	.883	0	.664
14		0	.729	0	.727	0	.753	0	.757	0	.746
15		6	.666	6	.655	6	.675	6	.675	3	.881
16		0	.728	0	.718	0	.740	0	.740	0	.736
17		3	.868	3	.848	3	.864	3	.857	0	.638
18		0	.677	0	.669	0	.689	0	.690	0	.681
19		6	.690	6	.684	6	.707	6	.711	3	.906
20		0	.715	0	.718	0	.745	0	.750	0	.745
21		0	.705	0	.699	0	.723	0	.726	0	.647
22		0	.657	0	.641	0	.655	0	.654	0	.588
23		0	.698	0	.694	0	.716	0	.719	0	.717
24		0	.691	0	.693	0	.720	0	.726	0	.822
25		0	.592	0	.595	0	.622	0	.631	0	.725
26		0	.709	0	.715	0	.745	0	.753	0	.756
27		0	.791	0	.797	0	.830	0	.838	0	.739
28		0	.700	0	.702	0	.731	0	.738	0	.657
29		0	.584	0	.579	0	.599	0	.601	0	.602
30		0	.686	0	.687	0	.711	0	.713	0	.810
31		0	.690	0	.690	0	.718	0	.722	0	.822
32		0	.580	0	.576	0	.601	0	.608	0	.615
33		0	.639	0	.623	0	.639	0	.637	0	.576
34		0	.735	0	.732	0	.757	0	.759	0	.686
35		0	.628	0	.636	0	.666	0	.676	0	.679
36		0	.567	0	.574	0	.603	0	.614	0	.695
37		0	.680	0	.685	0	.713	0	.719	0	.306

* Control rod insertion depth measured in active core layers (e.g., "6" = fully inserted, "0" = fully withdrawn, "2" = 33% inserted).

TABLE 5-7 (Sheet 2 of 2)
SUMMARY OF CONTROL ROD INSERTIONS AND AXIAL POWER FACTORS IN BOTTOM FUEL LAYER

	CYCLE	4		4		4		4	
	EFPD	200.0		250.0		295.0		300.0	
REGION									
1		2	.834	2	.826	2	.831	2	.791
2		0	.766	0	.761	0	.764	0	.726
3		0	.721	0	.714	0	.717	0	.678
4		0	.718	0	.704	0	.707	0	.667
5		0	.722	0	.706	0	.709	0	.668
6		0	.775	0	.767	0	.771	0	.732
7		0	.767	0	.763	0	.767	0	.729
8		0	.707	0	.707	0	.711	0	.674
9		0	.708	0	.710	0	.715	0	.678
10		0	.695	0	.690	0	.693	0	.655
11		3	.893	3	.878	3	.880	4	.878
12		0	.770	0	.757	0	.762	0	.723
13		0	.670	0	.658	0	.663	0	.625
14		0	.744	0	.731	0	.737	0	.698
15		3	.868	3	.850	3	.852	4	.845
16		0	.737	0	.733	0	.739	0	.701
17		0	.652	0	.654	0	.660	0	.624
18		0	.686	0	.686	0	.692	0	.657
19		3	.899	3	.893	3	.895	4	.896
20		0	.751	0	.751	0	.756	0	.718
21		0	.661	0	.664	0	.672	0	.638
22		0	.598	0	.601	0	.611	0	.580
23		0	.718	0	.715	0	.722	0	.684
24		0	.813	0	.803	0	.808	0	.767
25		0	.719	0	.709	0	.716	0	.675
26		0	.756	0	.747	0	.753	0	.713
27		0	.747	0	.739	0	.746	0	.708
28		0	.665	0	.658	0	.667	0	.632
29		0	.602	0	.596	0	.607	0	.572
30		0	.797	0	.782	0	.788	0	.747
31		0	.811	0	.801	0	.808	0	.767
32		0	.618	0	.620	0	.631	0	.596
33		0	.586	0	.591	0	.603	0	.573
34		0	.699	0	.704	0	.712	0	.679
35		0	.686	0	.690	0	.698	0	.661
36		0	.693	0	.694	0	.701	0	.662
37		0	.802	0	.798	0	.802	0	.763

LCO 4.1.3 limits: Fully inserted or fully withdrawn: 0.90
Partially inserted: 1.23

TABLE 5-8

RATIO OF FLUX LEVEL IN CENTER OF CORE TO AVERAGE CORE

FLUX LEVEL AT LOWER POWER LEVELS

Number of Rods Inserted*	Flux Ratio
19	1.15
22	1.33
25	1.03

* See Table 5-6.

TABLE 5-9

CONTROL ROD BANK WORTH

	Cycle 4 BOC(a)	MOC	EOC
Total bank worth, Δk (37 rod pairs inserted)	0.215	0.216	0.217
Total bank worth, Δk, less maximum worth rod pair	0.175	0.167	0.161
Total bank worth, Δk, less two maximum worth rod pairs	0.135	0.133	0.130
Total bank worth, Δk, less three inoperable rod pairs	N/A(b)	0.131	0.128

(a) Xenon assumed at equilibrium at 5EFPD.

(b) Pa-233 is not equilibrated at BOC; thus, the three rod criterion of LCO 4.1.2 is not applicable.

TABLE 5-10

SHUTDOWN MARGINS - CYCLE 4

Number of Inoperable Rods	Shutdown Margin, Δk		
	BOC[a]	MOC	EOC
0[b]	0.085	0.096	0.114
1[b]	0.042	0.043	0.054
2[c]	0.011	0.031	0.046
2[d]	N/A[e]	0.030	0.046
3[d]	N/A[e]	0.028	0.045

(a) Xenon assumed at equilibrium at 5EFPD, 60 days prior refueling outage.

(b) Core at room temperature with complete Pa-233 decay.

(c) Core at refueling temperature with two-week Pa-233 decay.

(d) Core at room temperature with no Pa-233 decay.

(e) Pa-233 is not equilibrated at BOC; thus, the two rod and three rod criteria of LCO 4.1.2 are not applicable.

NOTE: General requirements for operability of control rod drives during the cycle are provided in Technical Specification LCO 4.1.2.

TABLE 5-11

KINETICS PARAMETERS

	Initial Core		Cycle 4		Equilibrium Cycle	
	BOC, with Xe	EOC	BOC, with Xe	EOC	BOC, with Xe	EOC
Fractional productions						
From U-233	0.0	0.19	0.33	0.48	0.38	0.48
From U-235	1.0	0.81	0.67	0.52	0.62	0.52
Prompt neutron lifetime, sec						
Hot	2.69×10^{-4}	3.17×10^{-4}			2.85×10^{-4}	3.41×10^{-4}
Cold	2.43×10^{-4}	2.81×10^{-4}			2.64×10^{-4}	3.09×10^{-4}
Effective delayed neutron fraction	0.00650	0.00577	0.00522	0.00465	0.00505	0.00451
Delayed neutron decay constant, λ, sec^{-1}						
Precursor 1	0.01243	0.01249	0.01249	0.01252	0.01250	0.01251
2	0.03050	0.03088	0.03120	0.03160	0.03126	0.03164
3	0.1114	0.1136	0.1171	0.1204	0.1170	0.1199
4	0.3013	0.3025	0.3044	0.3064	0.3047	0.3068
5	1.136	1.136	1.135	1.135	1.135	1.135
6	3.013	2.981	2.940	2.892	2.913	2.859
Delayed neutron fraction, β						
Precursor 1	0.000214	0.000219	0.000219	0.000222	0.000220	0.000222
2	0.001424	0.001	0.001214	0.001121	0.001186	0.001099
3	0.001274	0.001	0.001073	0.000983	0.001046	0.000961
4	0.002568	0.00	0.001956	0.001685	0.001874	0.001619
5	0.000748	0.0005	0.000543	0.000452	0.000516	0.000430
6	0.000273	0.0002	0.000212	0.000185	0.000204	0.000179

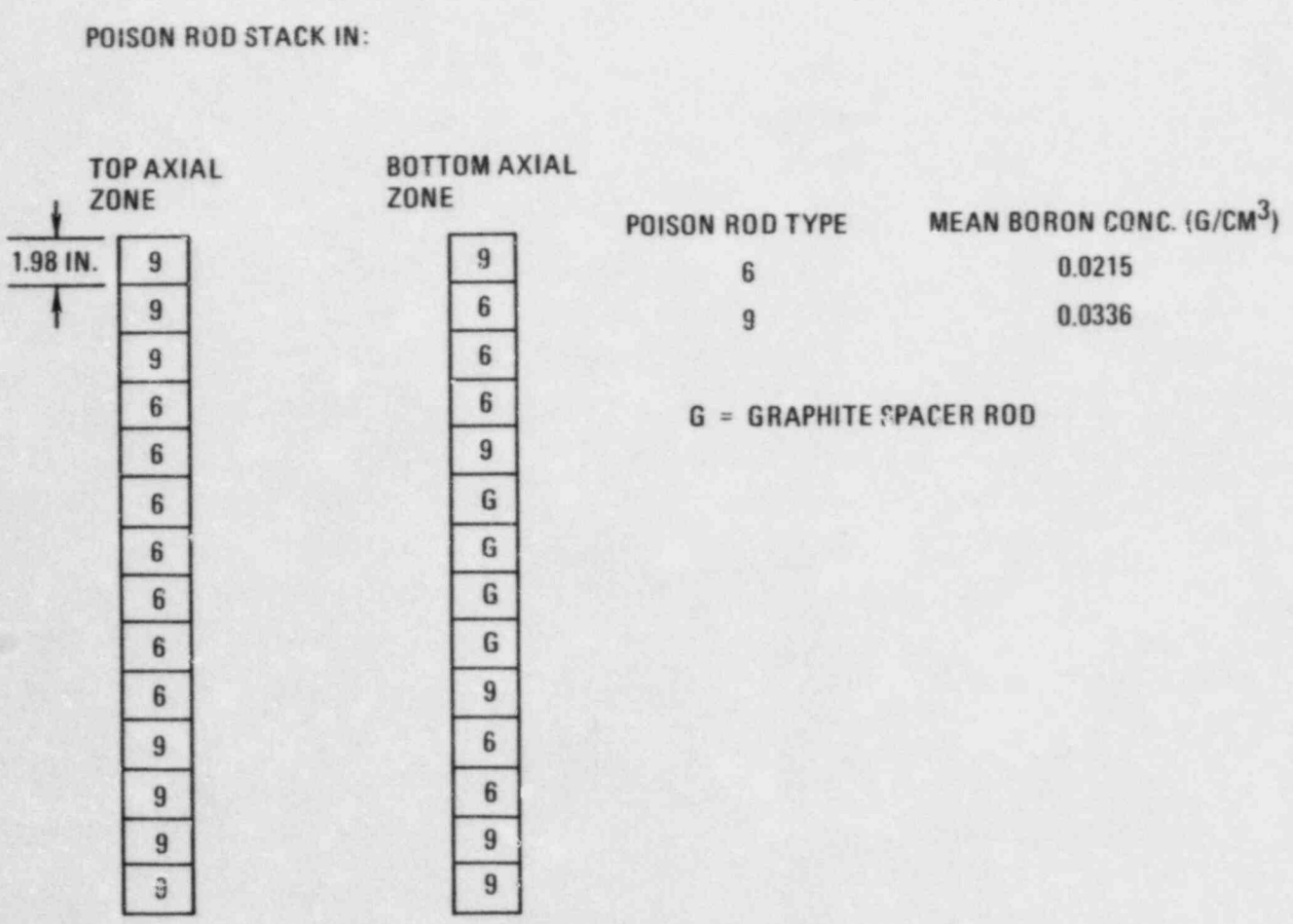

Fig. 5-1. Segment 8 poison rod using surplus Segment 7 LBP rods

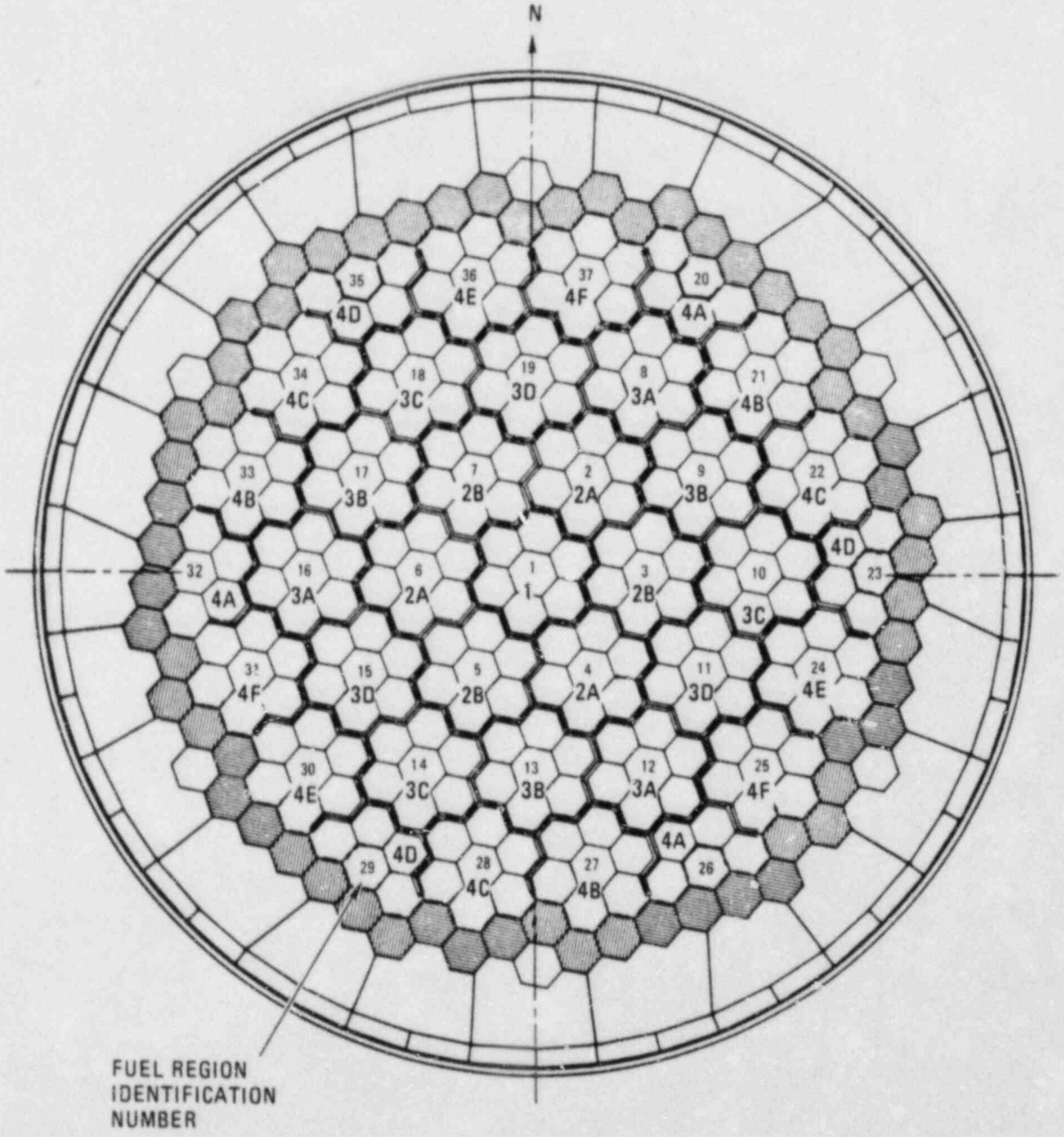

Fig. 5-2. Identification of control rod groups

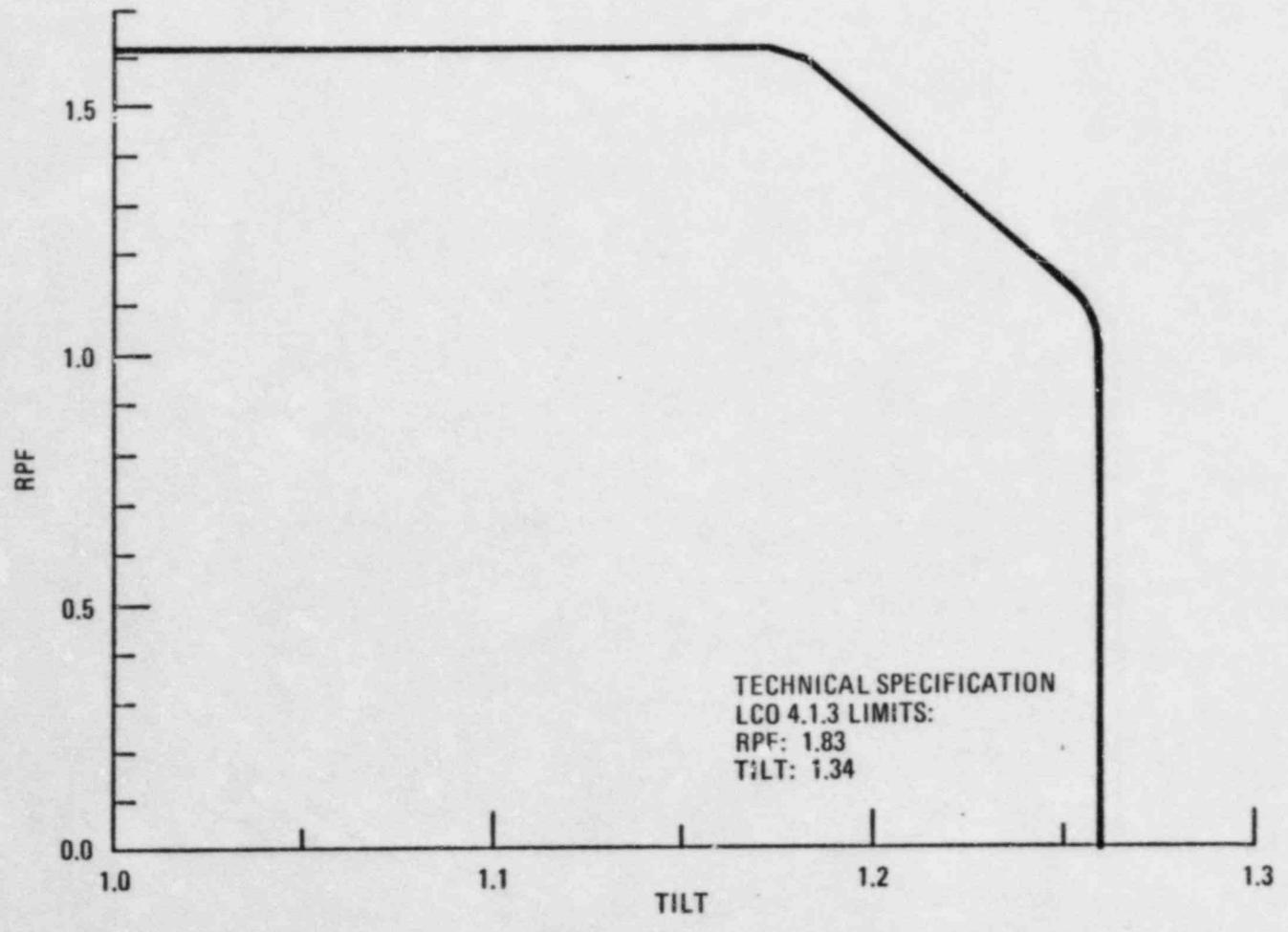

Fig. 5-3. Tilt envelope for Cycle 4: (a) unrodded regions

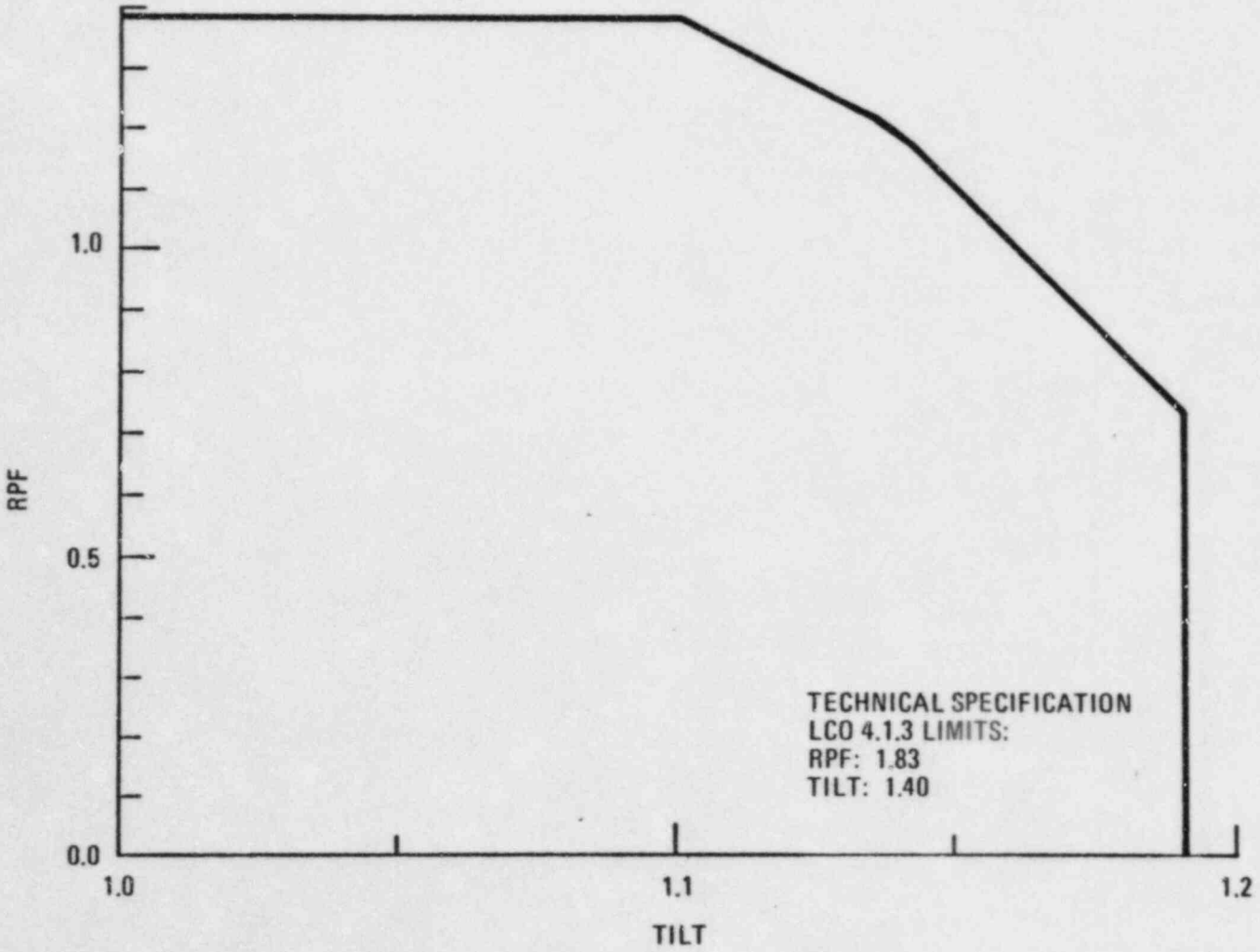

Fig. 5-3. Tilt envelope for Cycle 4: (b) partially rodded regions

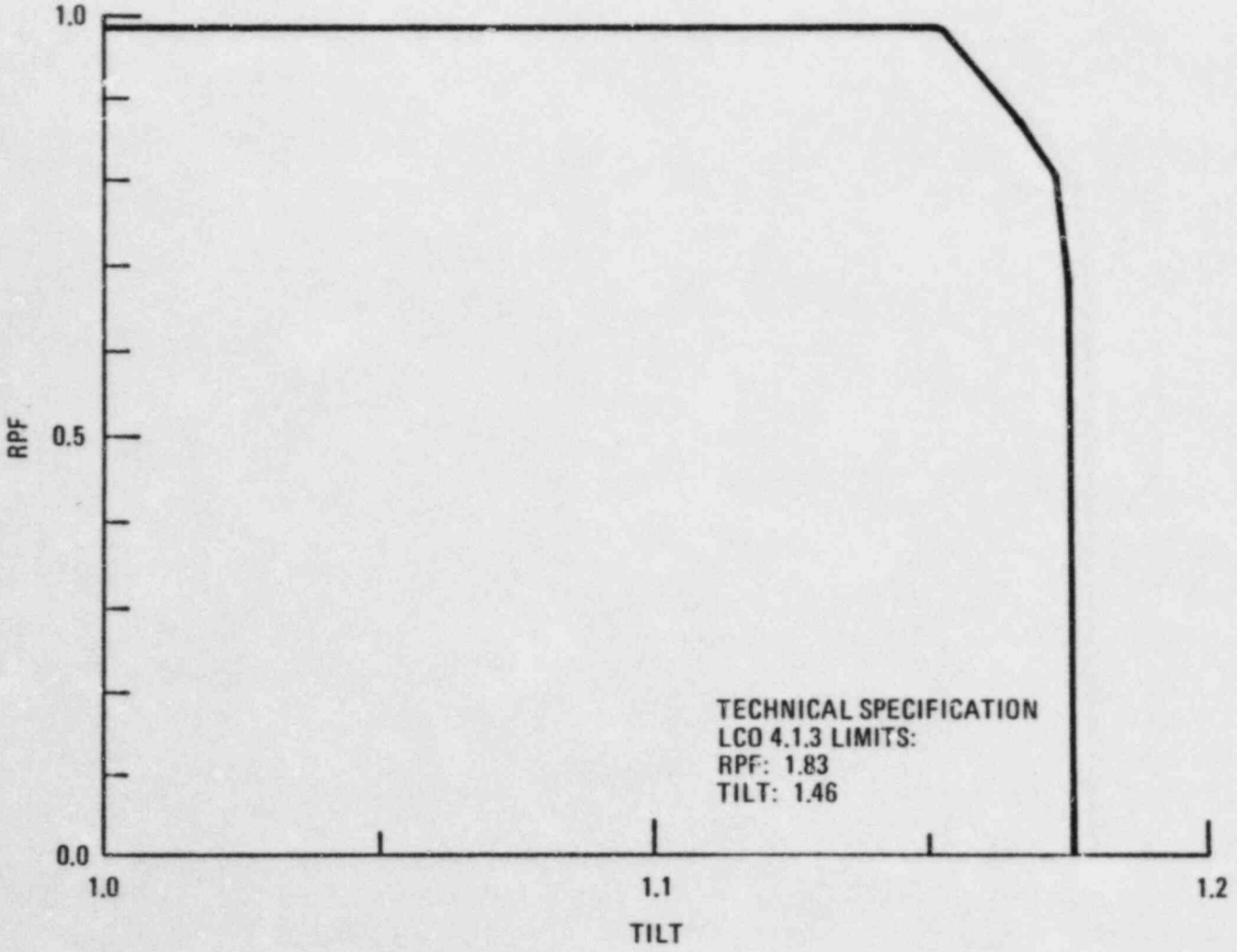

Fig. 5-3. Tilt envelope for Cycle 4: (c) fully rodded regions

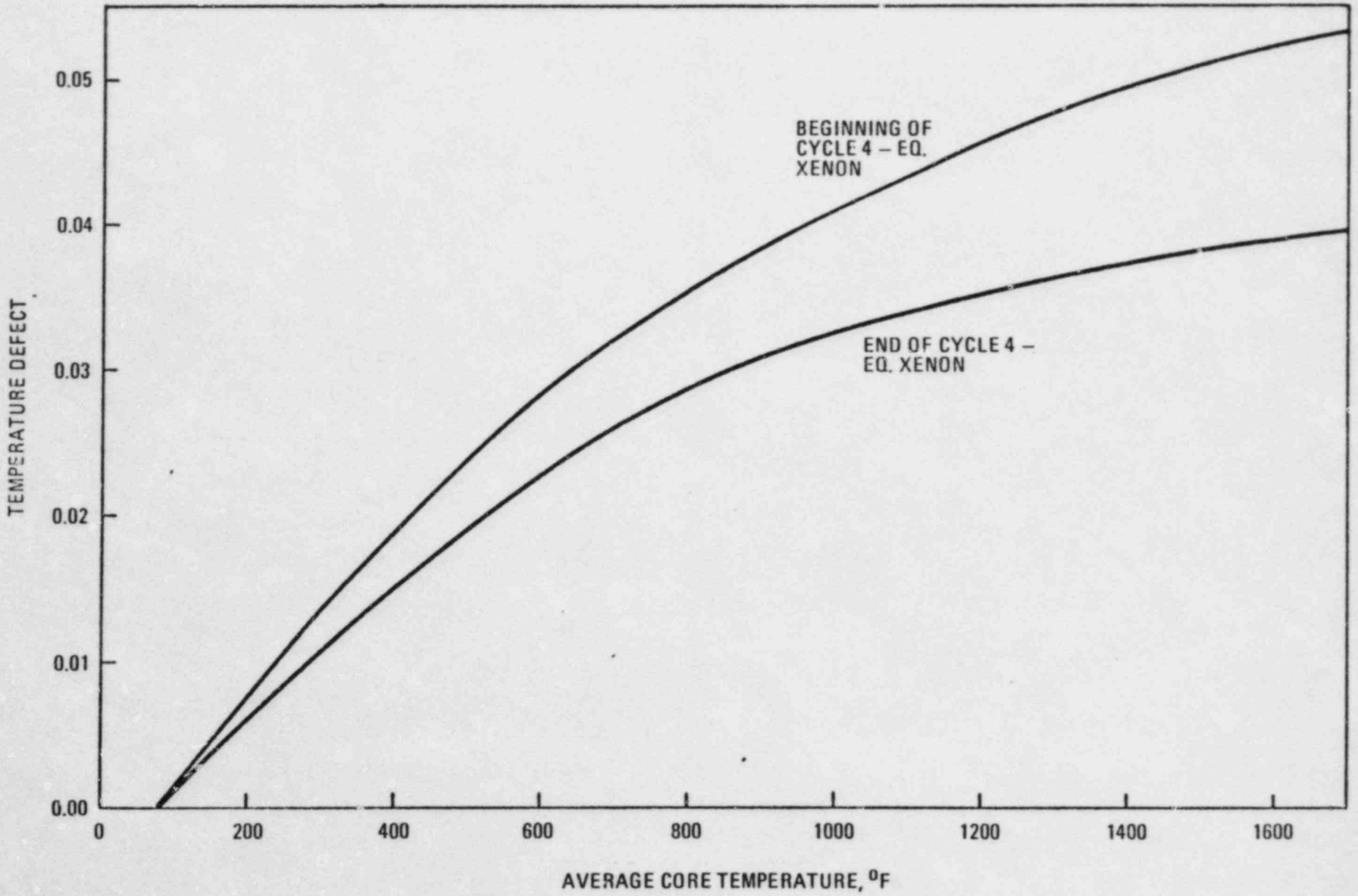

Fig. 5-4. Temperature defect vs. average core temperature

6. THERMAL-HYDRAULIC DESIGN

As noted in Section 4.3, the thermal design of the Segment 9 fuel elements is essentially the same as that of the initial core. No changes have been made in fuel element geometry. The power distributions expected during the fourth cycle are within the envelopes defined by Technical Specification LCO 4.1.3. Hence, except for the opening of cross-flow gaps, as discussed and accounted for in Section 3.6.2.2 of the original and updated FSARs, core coolant flow characteristics are also unaffected. Accordingly, there are no changes in the thermal-hydraulic design limits of the Segment 9 fuel elements from those of the initial core or the equilibrium core.

During Cycle 4, the core pressure drop will continue to increase toward the design equilibrium core value of 8.4 psid. Maximum core pressure drop during Cycle 4 is expected to be about 6.3 psid.

7. SAFETY ANALYSIS

7.1 INTRODUCTION AND SUMMARY

In this section, events and accidents previously analyzed in Chapter XIV of the Fort St. Vrain FSAR are reviewed to determine if the loading of Segment 9, which uses H-451 graphite, in FSV could alter the likelihood or consequences of postulated accidents. The purpose of such a review is to assure that the worst case conditions previously defined for accident analyses, and found to be acceptable during the FSAR review, are not exceeded and that no unreviewed safety questions are presented.

Chapter XIV of the FSAR has been examined to identify those events which might be affected by the insertion of fuel elements of H-451 graphite into the core. The results of this examination are given in Table 7-1. Those events which require a more detailed examination are:

1. Rod withdrawal accidents (RWAs).
2. Fuel element malfunctions.
3. Loss of normal shutdown cooling (limiting case: cooldown on one firewater-driven circulator).
4. Moisture inleakage.
5. Permanent loss of forced circulation (DBA #1).
6. Rapid depressurization/blowdown (DBA #2).

As indicated in Table 7-1, RWAs and fuel element malfunctions are discussed in Sections 5.5 and 4.2 of this document, respectively. It is concluded in Section 5.5 that the neutronic consequences of a RWA will be unchanged, and that RWA consequences are no more severe than

those of the postulated RWA described in the FSAR. For "Fuel Element Malfunction," the H-451 graphite fuel elements will experience less stress buildup than some H-327 graphite fuel elements in Segment 9, and as discussed in Reference 7 the strength of H-451 graphite is higher than that of H-327. The consequences of fuel element malfunction are no more severe than those described in the FSAR. Thus, a larger safety margin against this accident is provided. This result is consistent with the conclusions reached in References 8-16.

In the sections which follow, it is demonstrated for the remaining events (i.e., items 3 through 6) that existing FSAR results of accident analyses conservatively bound any perturbations resulting from the introduction of H-451 graphite fuel elements. These results are also consistent with conclusions reached in References 8-16.

7.2 LOSS OF NORMAL SHUTDOWN COOLING

Loss of normal shutdown cooling is discussed in Section 14.4 of the FSAR. The limiting case (Section 14.4.2.1, Case B2) of this event was determined to be cooling with one circulator driven by the firewater system.

As shown in Section 5, the introduction of H-451 graphite fuel elements in Segment 9 introduces no adverse changes in core neutronics values used in FSAR analysis of this accident. Specifically, no adverse impact on power peaking factors is created (Section 5.3), there is no adverse impact on power distribution (Section 5.4), core shutdown margins are not adversely affected (Section 5.6), and kinetic parameters are not adversely affected (Section 5.7). In addition, since the thermal properties of H-451 graphite are the same or better than those of H-327 graphite (Ref. 8), the heat transport analyses in the FSAR are not adversely affected.

Therefore, as there are no changes required for either the neutronic or thermal conditions employed in the FSAR analysis of this accident, the FSAR conclusions regarding this accident are not invalidated by the use of H-451 graphite fuel elements in Segment 9.

7.3 MOISTURE INLEAKAGE

The analysis in Section 14.5.2 of the FSAR considers inleakage into the primary coolant system from an economizer-evaporator-superheater subheader or tube or from the helium circulator bearing water supply.

Of the moisture ingress cases treated in the FSAR, Case 5, a steam generator subheader rupture compounded by concurrent failure of the moisture monitor system and dumping of the wrong (non-leaking) steam loop, has the greatest potential for graphite oxidation and fuel hydrolysis in the shortest time following the accident. As shown in the FSAR, Cases 5 and 6 actually show comparable results. To evaluate the potential effect of the application of H-451 graphite in Segment 9 on the analysis of Case 5, the following phenomena were investigated:

1. Steam-graphite reaction.
2. Hydrolysis of failed fuel.
3. Potential change in fission product release due to (1) and (2).

7.3.1 Steam-Graphite Reactions

As shown in Figs. 6-1 and 6-2 of Reference 19, the steam-graphite reaction rates at various temperatures for H-327 and H-451 are approximately equal within experimental uncertainty over the

temperature range of interest [700° to 1300°C (1292° to 2372°F)]. Furthermore, the reaction dependence on fractional graphite burnoff is not particularly sensitive to the change in graphite type. Hence, the same reaction rate equations have been recommended for both types of graphite.

Since the thermal conductivity of H-451 is somewhat higher than that of H-327, graphite temperatures will be somewhat lower, tending to reduce reaction rates. In addition, since Segment 9 contains reference fuel, catalyst (barium and strontium) concentrations in the fuel blocks will remain within the conservative values already used to calculate the effect of these catalysts. Thus, for a given inleakage of steam or water into the primary coolant system, the amount of core graphite which reacts will be approximately the same for either type of graphite. Accordingly, the production of CO and H_2 during the moisture ingress events will be approximately the same and, thus, primary coolant system pressure rise during moisture ingress will also be approximately equal for either graphite.

7.3.2 Hydrolysis of Failed Fuel

Hydrolysis of failed fuel can result in the release of an additional fraction of the noble gas fission product inventory from the core to the primary coolant system. However, since the primary coolant system remains essentially leak tight after a steam leak accident, this release represents no hazard to the general public.

The hydrolysis reaction with fuel particles occurs only when steam diffuses through the graphite block and reacts with fuel kernels having coatings that failed prior to the moisture ingress event. The rate of hydrolysis and associated release of noble gas fission products is dependent upon local fuel temperatures and steam concentration.

As noted in Section 4.3, the increased thermal conductivity of H-451 will result in somewhat lower fuel temperatures. Thus, the magnitude of fuel coating failures considered in the FSAR for moisture ingress events should conservatively bound those estimates after the substitution of H-451 graphite.

The slightly lower fuel element graphite temperatures will have only a small effect on the graphite reaction and corresponding depletion of steam concentration; thus, the extent of the fuel hydrolysis reaction during moisture ingress events is expected to be nearly the same for the H-451 graphite in Segment 9 as that predicted for the H-327 graphite which it replaces. Therefore, the hydrolysis of failed fuel and concurrent noble gas release would be essentially the same for the H-451 elements and would be bounded by the FSAR analysis. Further detailed discussion of graphite oxidation and failed fuel hydrolysis, and of the interaction between these phenomena, can be found in Reference 10.

7.3.3 Fission Product Release from Oxidized Graphite

The amount of activity released to the primary coolant system from oxidized graphite is proportional to the amount of graphite reacted and the concentration of fission products within that graphite. The fission product retention characteristics of H-451 graphite are similar to H-327 (Reference 10) and since no change in fuel failure characteristics is anticipated, the fission product concentration in the fuel blocks will be essentially unchanged after the substitution of H-451.

Thus, since the amount of graphite reacted is approximately the same for either type, the corresponding release of fission products will also be the same.

7.4 PERMANENT LOSS OF FORCED COOLING [Design Basis Accident No. 1(DBA-1)]

This hypothetical event assumes permanent loss of forced circulation of primary coolant helium. The FSAR considers consequences of this event in four categories:

1. Thermal results wherein metallic components might fail.

2. Structural results which might affect the core, reflector, core barrel, or core support structure.

3. Nuclear consequences which affect shutdown capability.

4. Fission product release and offsite doses.

Because the thermal properties of H-451 graphite are the same or better than those of H-327 graphite (Reference 8), the substitution of H-451 graphite in Segment 9 will not alter the thermal effects adversely, and the conclusion in the FSAR will remain unchanged.

The structural results mainly concern thermal stresses which might affect the structural integrity of the core support and lateral restraint. Such structural effects, external to the core, are not influenced by the nature of the fuel element graphite. In addition, there is little concern regarding the fuel blocks and reflector because during this accident, the maximum compressive load in these components is less than 140 kPa (20 psi) at the bottom of the core, and about half that at the hottest central core region. These loads are small compared with the graphite axial compressive stress. In addition, the strength of H-451 graphite is superior to that of H-327 (Reference 8).

The nuclear consequences concern reactivity effects whereby the potential reduction of shutdown margin in the overheated core could result from compaction and melting of control rods or spatial redistribution of control poison, fission product poisons, or uranium and thorium. The FSAR shows that these effects do not result in an increase in reactivity at any time during the accident. Since no change in fuel type is being considered, the Cycle 4 core is expected to perform quite similarly to the existing core with respect to fission product and fuel redistribution during a loss of forced cooling (LOFC) event. As discussed in Section 5, the presence of H-451 graphite in the core will not have a significant effect on reactivity.

The offsite doses for DBA-1, reported in Table 14.10-1 of the FSAR, are within the 10CFR100 guidelines even with the conservative assumption of TID-14844 release fractions. Because the fission product retention capabilities are similar to those for H-327, the substitution of H-451 graphite in Segment 9 will have a negligible effect on the fission product release characteristics during the core heat-up event and, hence, the FSAR conclusion regarding the event remains unchanged, as was also concluded in References 8-16.

7.5 RAPID DEPRESSURIZATION/BLOWDOWN (DBA-2)

The FSAR considers three classes of events for loss of primary coolant: primary coolant leakage (Section 14.7), maximum credible accident (Section 14.8), and the hypothetical DBA-2, "Rapid Depressurization/Blowdown" (Section 14.11). Since the third class envelopes any potential consequences of the other two, it alone was considered for possible impact by the H-451 graphite in Segment 9.

The aspects of a DBA-2, which are discussed in Section 14.11 of the FSAR, are as follows:

1. Integrity of reactor internals.
2. Continuation of adequate primary coolant circulation.
3. Ingress of air.
4. Effects of operator actions.
5. Vertical thrust on the PCRV.
6. Effect on building pressure.
7. Radiological consequences.

Item 1 concerns the pressure differentials that could develop across reactor components during the depressurization. Item 2 concerns the ability of the helium circulators to continue operation and provide adequate core cooling in the event of a PCRV penetration failure. These items obvioiusly are not affected by the presence of H-451 graphite in the core except for the fact that H-451 has higher strength and, therefore, has greater margins of safety under accident loadings.

Item 3 concerns the possible pathways for air ingress into the PCRV following a DBA-2. The FSAR shows that the operation of a helium purge flow would virtually exclude oxygen from entering the PCRV and that even if the purge were inoperative, the oxygen ingress would be insignificant with respect to heat generation and graphite combustion. Since the mechanical design of the PCRV and purge system is not being altered and the oxidation reaction rate with air is rapid and insensitive to catalytic effects and the type of graphite, the FSAR conclusions are not altered.

Regarding Item 4, the FSAR describes how automatic reactor scram and alarm would alert the operator to the fact that a leak has developed in the PCRV and to be ready to perform necessary monitoring and system adjustments. The operator's responsibilities are neither increased nor diminished by the presence of H-451 graphite in the core. Items 5 and 6 concern mechanical processes external to the PCRV and core. Therefore, only Item 7 needs to be further examined.

As discussed in the FSAR, the radiological release from a postulated DBA-2 consists of essentially all the activity which exists in the circulating primary coolant prior to the depressurization event plus a small fraction of the activity plated out on the surfaces of the primary circuit. Since the fission product transport and retention characteristics of the H-451 graphite are nearly identical to those of H-327 (Reference 10) the radiological consequences of this accident would be essentially unchanged from those reported in the FSAR.

7.6 CONCLUSIONS

A review of Chapter XIV of the FSAR identified six postulated accident conditions which required more detailed examination for potential impact from the substitution of H-451 graphite in Segment 9 for the fuel element block material. These accident conditions were discussed in this section and no requirement for additional analysis has been identified. It is concluded that the worst case conditions previously defined for accident analyses, and found to be acceptable during the FSAR review, are not exceeded as a result of introducing H-451 graphite in Segment 9. This result is consistent with the conclusions of References 8-16. This design change presents no unreviewed safety questions, as defined in 10CFR50.59.

TABLE 7-1
POTENTIAL EFFECTS OF CYCLE 4 ON FSV FSAR ACCIDENT PREDICTIONS

FSAR Chapter XIV Event	Potential Effects on Event Analysis Due to Application of H-451 Graphite
14.1 Environmental Disturbances	
Earthquake	Mechanical effects are discussed in Section 4.2. Any reactivity effect would be bounded by rod withdrawal events.
Wind effects, Flood, Fire, Landslides, Snow and Ice	The core is not affected by these events.
14.2 Reactivity Accidents and Transient Response	
Summary of reactivity sources	
Excessive removal of control poison; Loss of fission product poisons; Rearrangement of core components; Sudden decrease in reactor temperature	Reactivity insertions in these events are less than rod withdrawal events.
Rod withdrawal accidents	Evaluation required, see Section 5.5 of this document.
14.3 Incidents	
Incidents Involving the Reactor Core	
Column deflection & misalignment	No change from Sect. 3.3.1.2 of FSAR.
Fuel element malfuctions	Evaluation required, see Section 4.2 of this document.
Misplaced fuel element	No change from Sect. 3.5.4.5 of FSAR.
Blocking of coolant channel	No change from Sect. 3.6.5.2 of FSAR.
Control rod malfunctions	No change from Sect. 3.8 of FSAR.
Orifice malfunctions	No change from Sect. 3.6.5.1 of FSAR.
Core support floor loss of cooling	No change from Sect. 3.3.2.2 of FSAR.
Incidents Involving the Primary Coolant System	None

TABLE 7-1 (continued)
POTENTIAL EFFECTS OF CYCLE 4 ON FSV FSAR ACCIDENT PREDICTIONS

	FSAR Chapter XIV Event	Potential Effects on Event Analysis Due to Application of H-451 Graphite
	Incidents Involving the Control and Instrumentation System	None
	Incidents Involving the PCRV	None
	Incidents Involving the Secondary Coolant & Power Conversion System	None
	Incidents Involving the Electrical System	None
	Malfunctions of the Helium Purification System	None
	Malfunctions of the Helium Storage System	None
	Malfunctions of the nitrogen system	None
14.4	Loss of Normal Shutdown Cooling	Evaluation required, see Sect. 7.2 of this document.
14.5	Secondary Coolant System Leakage	
	Steam leaks outside the primary coolant system	None
	Leaks inside the primary coolant system/steam generator leakage (moisture ingress)	Evaluation required, see Sect. 7.3 of this document.
14.6	Auxiliary System Leakage	
	Failure involving the helium purification system	
	Loss of both purification trains	Possible effects would be bounded by Design Basis Accident No. 2, FSAR Section 14.11.
	Failure of regeneration line with simultaneous valve failure and operational error	
	Accidents involving the gas waste system	No change from Sect. 14.6.2 of FSAR.
	Fuel handling and storage accidents	
	Fuel handling accidents	No change from Sect. 14.6.3 of FSAR.
	Fuel storage accidents	

TABLE 7-1 (continued)
POTENTIAL EFFECTS OF CYCLE 4 ON FSV FSAR ACCIDENT PREDICTIONS

FSAR Chapter XIV Event		Potential Effects on Event Analysis Due to Application of H-451 Graphite
14.7	Primary Coolant Leakage	Possible effects would be bounded by Design Basis Accident No. 2, FSAR Sect. 14.11.
14.8	Maximum Credible Accident	
14.9	Maximum Hypothetical Accident	Same as FSAR Sect. 14.11
14.10	Design Basis Accident No. 1, "Permanent Loss of Forced Circulation (LOFC)"	Evaluation required, see Sect. 7.4 of this document.
14.11	Design Basis Accident No. 2, "Rapid Depressurization/ Blowdown"	Evaluation required, see Sect. 7.5 of this document.

8. PROPOSED MODIFICATIONS TO TECHNICAL SPECIFICATIONS

One change to the plant technical specifications is necessitated by the insertion of Segment 9 into the reactor core. Technical Specification DF6.1, Reactor Core Design Features, describes the overall design features of the reactor core which were used to evaluate its general performance. In the initial issue of the Technical Specifications, and at the time of the initial CA submittal to NRC on use of H-451 graphite in Fort St. Vrain (Ref. 8), Specification DF6.1 did not specify the graphite type used in fabrication of the fuel elements.

However, on May 25, 1979, four days after issuance of the NRC Safety Evaluation Report for H-451 graphite (Ref. 16), Amendment 20 to the FSV Operating License was issued by NRC. This amendment included a change to Technical Specification DF6.1 in which the composition of the eight test elements that were placed in the core during the first refueling is described. In the revised DF6.1 it was noted that the test elements are fabricated from H-451 graphite, while the reference fuel elements are fabricated from H-327 graphite.

Accordingly, it is proposed that Technical Specification DF6.1 be modified by inserting the following paragraph after the second paragraph on page 6.1-4:

"Beginning with core Segment 9 (Reload 3), H-451 near-isotropic graphite is used in the fabrication of reload fuel elements in addition to or in place of the previous reference H-327 needle coke (anisotropic) graphite."

9. STARTUP TESTS

Following refueling, a stepwise approach to full power will be performed. During these power steps, the following tests will be performed:

1. Differential control rod calibration measurements. These tests are required by Technical Specification SR 5.1.5. The method used for these measurements is the same as that in SUT B-9.

2. Temperature coefficient (temperature reactivity defect) measurements. This test is required by Technical Specification SR 5.1.3. The method used for these measurements is the same as that in SUT B-8.

3. Reactivity status surveillance check. This test is performed at each startup and once per week as required by Technical Specification SR 5.1.4.

In addition, as requested by NRC in the Safety Evaluation Report for Amendment 28 of the FSV Operating License, data taking procedures similar to those used in the RT-500K test series (Ref. 3) will be followed during the startup after refueling. These procedures will be used to characterize reactor performance at core pressure drops higher than the 5 psid level tested in previous testing up to 100% power. The procedures used and the data acquired will be provided to the NRC staff, for information, in one or more separate submittals.

10. REFERENCES

1. Burnette, R. D., "Radiochemical Analysis of the First Plateout Probe from the Fort St. Vrain High-Temperature Gas-Cooled Reactor," GA-A16764, June 1982, PSC letter to NRC P-82419, September 27, 1982.

2. Fuller, J. K. (PSC) letter to William P. Gammill (NRC), "SAR for Core Region Constraint Devices," P-79068, March 23, 1979.

3. Asmussen, K. E., et al., "Testing and Operation of Fort St. Vrain up to 100% Power," GA-C16701, June 1982, PSC letter to NRC P-82229, July 6, 1982.

4. Alberstein, D., and K. E. Asmussen, "Technical Specifications for Operation of FSV with Region Outlet Temperature Measurement Discrepancies," GA-C16781, June 1982, PSC letter to NRC P-82229, July 6, 1982.

5. Brey, H. L. (PSC) letter to George Kuzmycz (NRC), "Status of Cracked Fuel Element Webs," P-82394, September 15, 1982.

6. Fuller, J. K. (PSC) letter to William P. Gammill (NRC), "Extension of Cycle 2 (Reload 1) Operation," P-79025, January 25, 1979.

7. Swart, F. E. (PSC) letter to George Kuzmycz (NRC), "Safety Analysis Report for Fuel Reload 2 (Cycle 3) - Preliminary," P-81012, January 13, 1981.

8. "Safety Analysis Report: Use of H-451 Graphite in Fort St. Vrain Fuel Elements," GLP-5588, December 20, 1977, G. L. Wessman (GA) letter to R. P. Denise (NRC), March 28, 1978.

9. Speis, Themis P. (NRC) letter to G. L. Wessman (GA), "Request for Additional Information on H-451," September 19, 1978.

10. Wessman, G. L. (GA) letter to William Gammill (NRC), October 30, 1978.

11. Wessman, G. L. (GA) letter to William Gammill (NRC), November 17, 1978.

12. Speis, Themis P. (NRC) letter to George Wessman (GA), "Request for Additional Information on H-451 Graphite," January 10, 1979.

13. Speis, Themis P. (NRC) letter to George Wessman (GA), "Additional Information Request on H-451 Graphite," February 5, 1979.

14. Wessman, G. L. (GA) letter to William Gammill (NRC), February 6, 1979.

15. Wessman, G. L. (GA) letter to William Gammill (NRC), February 15, 1979.

16. Gammill, William P. (NRC), letter to Colin Fisher (GA), "Evaluation of Topical Report GLP-5588", May 21, 1979.

17. Brey, H. L. (PSC) letter to Phillip C. Wagner (NRC), "H-451 Graphite Status," P-83033, January 28, 1983.

18. Katz, R., and G. R. Malek, "COPE, a Core Performance Code for Gas-Cooled Reactors," GA-9802, November 15, 1969.

19. Engle, G. B., *et.al.*, "Development Status of Near-Isotropic Graphites for Large HTGRs," GA-A12944, June 1, 1974.

GA Technologies Inc.
P.O. BOX 81608
SAN DIEGO, CALIFORNIA 92138

ATTACHMENT 3

AMENDMENT 1 TO GLP-5588

P-83371

GA Technologies Inc.
P.O. BOX 85608
SAN DIEGO, CALIFORNIA 92138
(619) 455-3000

LRS:77:CRF:83
November 2, 1983

Director of Nuclear Reactor Regulation
U.S. Nuclear Regulatory Commission
Washington, DC 20555

Dear Sir,

In May 1979 the NRC staff completed its review of GA Technologies (formerly General Atomic Company) topical report GLP-5588, "Safety Analysis Report: Use of H-451 Graphite in Fort St. Vrain Fuel Elements." Upon completion of its review, the staff determined that GLP-5588 may serve as an acceptable reference and the initial basis for allowing substitution of near-isotropic H-451 graphite fuel and reflector elements for the current reference needle-coke H-327 graphite elements in Fort St. Vrain (Ref. 1).

In recent correspondence with Public Service Company of Colorado (Ref. 2), the NRC staff requested additional information regarding use of H-451 graphite in Fort St. Vrain. In part, these questions were prompted by the development of new models for irradiation-induced creep in graphite. The staff requested that GLP-5588 be amended to contain this new information.

Accordingly, enclosed are fifty (50) copies of Amendment 1 to GLP-5588. This amendment contains new information on irradiation-induced creep and irradiation-induced dimensional change both in H-451 and in H-327 graphite. The amendment is being submitted by GA Technologies, as noted in PSC's response to the NRC request for additional information (Ref. 3), because GLP-5588 is a GA topical report, the review of which was not part of the Fort St. Vrain licensing docket.

If you have any questions regarding this amendment, please feel free to call me at (619) 455-3821.

Very truly yours,

C. R. Fisher,
Manager - Licensing,
Reliability and Systems

Enclosure
cc: J. T. Collins, Region IV
M. Tokar, Core Performance Branch
P. C. Wagner, Region IV

References:

1. Gammill, William P. (NRC), letter to Colin R. Fisher (GA), "Evaluation of Topical Report GLP-5588," May 21, 1979.

2. Madsen, G. L. (NRC), letter to O. R. Lee (PSC), August 2, 1983.

3. Brey, H. L. (PSC), letter to John T. Collins (NRC), "Additional Information on H-451 Graphite," P-83348, October 27, 1983.

AMENDMENT INCORPORATION INSTRUCTIONS

GLP-5588 AMENDMENT 1

Delete Pages	Replace With Amendment Pages
iii, iv	iii, iv
4-1, 4-2	4-1, 4-2
4-3, 4-4	4-3, 4-3a; 4-4
4-7, 4-8	4-7, 4-8
4-9, 4-10	4-9, 4-10
4-11, 4-12	4-11, 4-12
4-17, 4-18	4-17, 4-18
4-21, 4-22	4-21, 4-22
4-25, 4-26	4-25, 4-26

CONTENTS

4. MATERIALS PROPERTY DATA

Determination of the material properties of nuclear-grade graphite is a continuing program at GA Technologies. The most recent values of H-451 and H-327 graphite material properties are given in Sections 4.1 and 4.2, respectively. 1

4.1. H-451 GRAPHITE MATERIALS PROPERTY DATA

4.1.1. Specific Heat

The specific heat of H-451 graphite over the temperature range 0° to 2700°C is given by Eq. 4-1, which is accurate to ±5% of the mean (Ref. 4-1):

$$C_p = 0.54212 - 2.42667 \times 10^{-6}\, T - 90.2725\, T^{-1} - 4.34493 \times 10^{4}\, T^{-2} + 1.59309 \times 10^{7}\, T^{-3} - 1.43688 \times 10^{9}\, T^{-4}. \quad (4\text{-}1)$$

4.1.2. Bulk Density

The mean bulk density for the H-451 log is 1.74 Mg/m^3 (Ref. 4-2).

4.1.3. Irradiation-Induced Dimensional Change (Refs. 4-3, 4-8, 4-9)

The permanent strain (ε°) due to irradiation-induced dimensional change has been expressed in terms of average irradiation temperature (T) and fast neutron fluence (ϕ) for near-isotropic graphite. The irradiation strain (ε°) is expressed by the polynomial in Eq. 4-2, which is valid for 1

4.1.7. Poisson's Ratio

The Poisson's ratio (ν) for H-451 graphite subjected to tensile strain is given as (Ref. 4-4)

$$\nu = 0.118\ (\pm 0.01).$$

4.1.8. Irradiation Creep Behavior

Irradiation-induced creep for both tensile and compressive stresses in near-isotropic graphite is described by Eq. 4-3 (Refs. 4-5a, 4-5b):

Irradiation temperature $\leq$ 650°C:

$$\varepsilon_{cr} = \frac{\sigma}{E}\left[1 - \exp\left(-2.5 \times 10^{-20}\ \phi\right)\right] + \frac{1.6 \times 10^{-21}\ \sigma E^{*}}{E_o}\int_o^{\phi} \frac{d\phi}{E(\phi,T)}$$

Irradiation temperature $>$ 650°C:

$$\varepsilon_{cr} = \frac{\sigma}{E}\left[1 - \exp\left(-2.5 \times 10^{-20}\phi\right)\right] + \frac{\sigma E^{*}\left[1.6 \times 10^{-21} + 5 \times 10^{-28}\ (T-650)^{2.6}\right]}{E_o}\int_o^{\phi} \frac{d\phi}{E(\phi,T)} \qquad (4\text{-}3)$$

where ε_{cr} = total uniaxial creep strain (cm/cm)

σ = stress (MPa)

E = Young's modulus when load is applied or changed (MPa)

ϕ = fast neutron fluence, n/cm^2 (E > 0.18 MeV, HTGR spectrum)

E^{*} = Young's modulus at a fluence of 1.4 x 10^{21} n/cm^2 (MPa)

4.1.10. Thermal Conductivity

The thermal conductivity of near isotropic graphite is given by the model of R. Price (Ref. 4-6). This model considers the dependence of thermal conductivity (K) on the current measurement temperature (T_c) and on the past history of irradiation temperature (T_1) and fast neutron fluence (ϕ). The model is extended here to the case of a nonisothermal irradiation with unknown temperatures.

The thermal conductivity as a function of current measurement temperature can be considered as a superposition of three temperature-dependent resistance mechanisms through the equation

$$K(T_c) = \frac{1}{\alpha\left[\frac{1}{K_U(T_c)} + \frac{1}{K_b'(T_c)} + \frac{d}{K_D'(T_c)}\right]}, \qquad (4\text{-}4)$$

where α is a porosity-tortuosity factor,

$K_U(T_c)$ is the crystallite conductivity with Umklapp processes dominating,

$b = 1/L_a$ (Ref. 4-6) is the inverse of the crystallite boundary spacing,

$K_b'(T_c) = (K_B/L_a)(T_c)$ (Ref. 4-6) is the effect of the grain boundary scattering

$d = C_d S_V^2$ (Ref. 4-6) is an irradiation damage parameter,

$K_d'(T_c) = (K_D C_D S_V^2)(T_c)$ (Ref. 4-6) is the effect of the irradiation damage.

All of the above quantities are given as known input data in Tables 4-5 and 4-6 with one exception: the irradiation damage parameter, d. As will be shown, one can solve for the parameter d by comparing conductivities before and after irradiation.

4.1.10.1. Thermal Conductivity, Unirradiated. For unirradiated material, the damage parameter d in Eq. 4-4 is zero. Equation 4-4 reduces to

where C_p = specific heat at constant pressure (cal/g-K),

T = temperature (K).

4.2.2. Bulk Density

The mean bulk density for the H-327 log is 1.77 Mg/m^3 (Ref. 4-7).

4.2.3. Irradiation-Induced Dimensional Change

The permanent strain (ε°) due to fast neutron damage in graphite has been measured in many experiments over the past 10 years. The irradiation strain in H-327 graphite is expressed as a polynomial for design use:

$$\varepsilon^\circ = (C_1 + C_2T + C_3T^2 + C_4T^3 + C_5T^4)\,\Phi + (C_6 + C_7T + C_8T^2 + C_9T^3 + C_{10}T^4 + C_{16}T^5)\,\Phi^2 + (C_{11} + C_{12}T + C_{13}T^2 + C_{14}T^3 + C_{15}T^4 + C_{17}T^5 + C_{18}T^6)\,\Phi^3, \quad (4\text{-}11)$$

where ε° = irradiation strain (dimensional change, $\Delta\ell/\ell$) (%),

Φ = fast neutron fluence (10^{25} n/m^2) $(E \geq 29\ fJ)_{HTGR}$,

T = average irradiation temperature (°C),

C_i = coefficients determined for each orientation of H-327 graphite; coefficients listed in Table 4-7.

The H-327 irradiation strain polynomial is based on data taken from the CG-1, -2, and -3 experiments and from experiments by ECN, Petten, in the Petten low temperature graphite capsules (Refs. 4-3, 4-8, 4-9). Irradiation strain (ε°) calculated from the above polynomial is valid for irradiation temperatures from 350° to 1000°C and fast neutron fluences of 0 to 8 x 10^{25} n/m^2 $(E \geq 29\ fJ)_{HTGR}$. The dimensional change in H-327 is shown in Fig. 4-5.

4.2.9. Thermal Expansivity

Figure 4-8 presents the design curve of thermal strain versus temperature for unirradiated H-327 graphite. The data of Fig. 4-6 are tabulated in Table 4-10.

4.2.10. Thermal Conductivity

The thermal conductivity of H-327 graphite is calculated using the previously described methodology for H-451 graphite conductivity (Section 4.1.10). The material constants for H-327 graphite to be substituted for Table 4.6 are given in Table 4-11. A plot of the thermal conductivity of H-327 graphite as a function of fast fluence and temperature is given in Fig. 4-7.

4-8. Price, R. J. and L. A. Beavan, "Final Report on Graphite Irradiation Test OG-1," USAEC Report GA-A13089, General Atomic Company, August 1, 1974, pp. 13 through 51.

4-9. Price, R. J. and L. A. Beavan, "Final Report on Graphite Irradiation Test OG-3," ERDA Report GA-A14211, General Atomic Company, January 1977, pp. 5-1 and 5-4.

4-10. Final Safety Analysis Report, Fort St. Vrain, Appendix F.

4-11. Price, R. J., "Mechanical Properties of Graphite for High Temperature Gas-Cooled Reactors: A Review," ERDA Report GA-A13524, General Atomic Company, September 22, 1975, pp. 2-6 through 2-9.

TABLE 4-7
COEFFICIENTS FOR IRRADIATION STRAIN POLYNOMIAL, H-327 GRAPHITE

	Axial	Radial
C_1	-5.108481	-0.309218
C_2	$+0.292901 \times 10^{-1}$	$+0.126366 \times 10^{-2}$
C_3	-0.644452×10^{-4}	-0.461461×10^{-5}
C_4	$+0.637722 \times 10^{-7}$	$+0.786252 \times 10^{-8}$
C_5	$-0.237075 \times 10^{-10}$	$-0.414299 \times 10^{-11}$
C_6	+2.977696	+1.417139
C_7	-0.189175×10^{-1}	-0.949423×10^{-2}
C_8	$+0.430617 \times 10^{-4}$	$+0.227745 \times 10^{-4}$
C_9	-0.422337×10^{-7}	-0.234320×10^{-7}
C_{10}	$+0.150559 \times 10^{-10}$	$+0.861987 \times 10^{-11}$
C_{11}	-0.268576	-0.147822
C_{12}	$+0.165487 \times 10^{-2}$	$+0.100726 \times 10^{-2}$
C_{13}	-0.369364×10^{-5}	-0.243819×10^{-5}
C_{14}	$+0.357371 \times 10^{-8}$	$+0.250028 \times 10^{-8}$
C_{15}	$-0.126622 \times 10^{-11}$	$-0.907074 \times 10^{-12}$
C_{16}	0	0
C_{17}	0	0
C_{18}	0	0

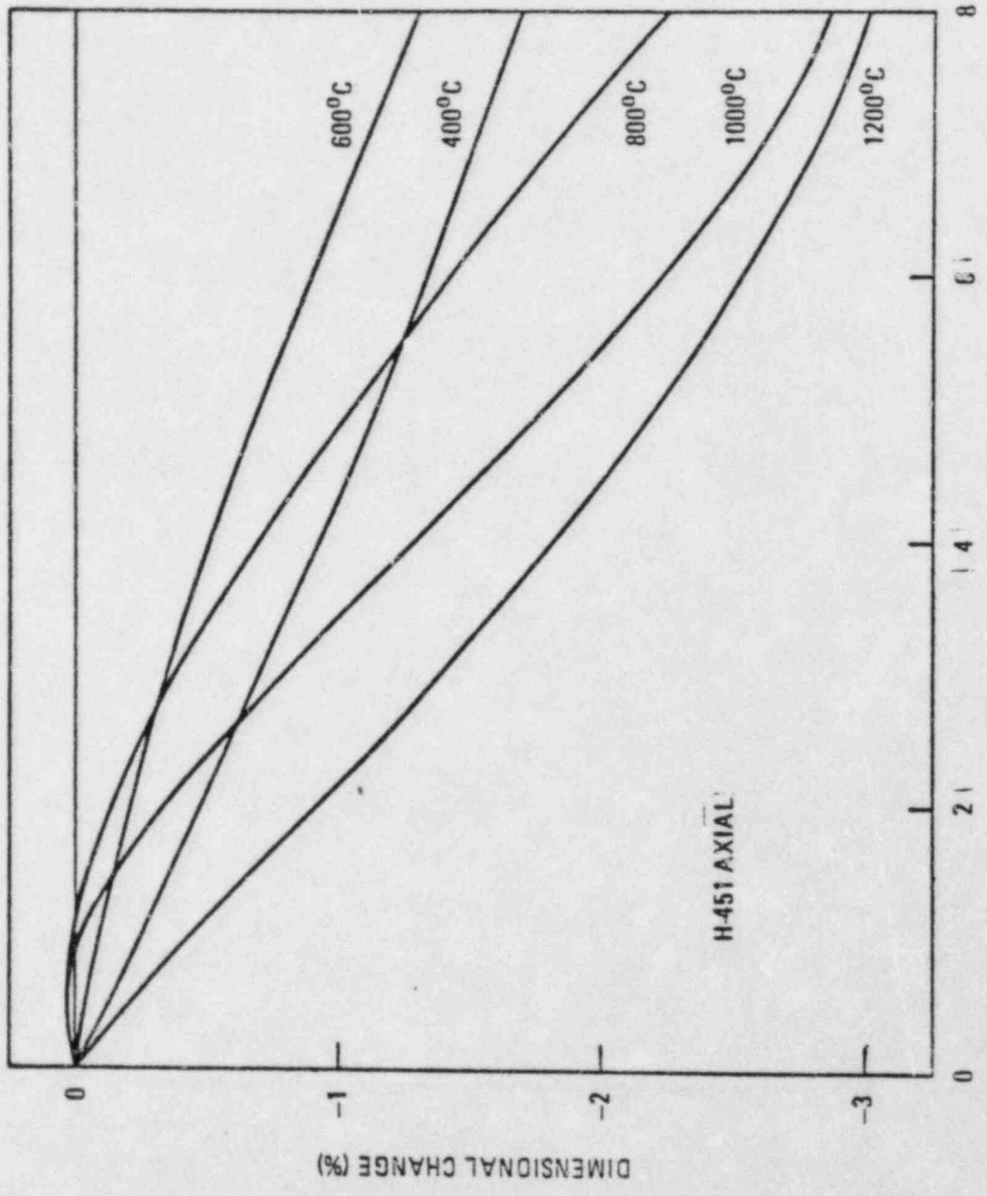

Fig. 4-1. Irradiation strain versus fast neutron fluence and irradiation temperature in H-451 near-isotropic graphite; axial orientation, calculated by using Eq. 4-2.

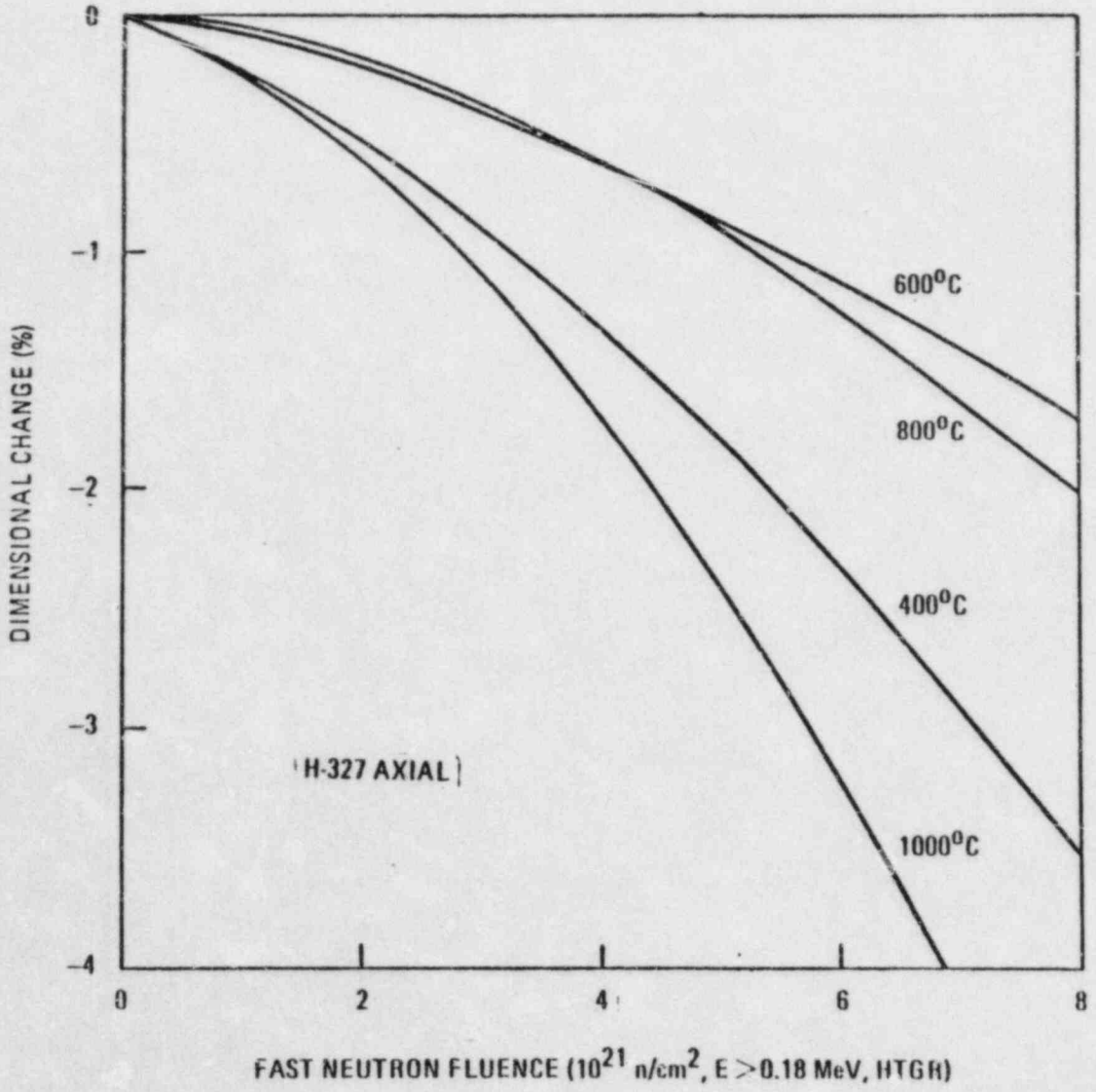

Fig. 4-5. Irradiation-induced dimensional change: (a) H-327, axial.